AN INVESTIGATION OF LEAD ZIRCONATE TITANATE THICK FILM ACTUATORS FOR MICRO-STRUCTURED OPTICAL ARRAYS

by

SHUANG LIU

A thesis submitted to the

University of Birmingham

for the degree of

MSc by Research

School of Metallurgy and Materials

College of Engineering and Physical Sciences

University of Birmingham

January 2013

An Investigation of Lead Zirconate Titanate Thick Film Actuators for Micro-structure Optical Arrays

Shuang Liu

Abstract

Micro-structured optical arrays (MOAs) are micro channels etched in silicon substrates and can be used as mirrors to reflect and focus X-rays. Piezoelectric PZT (lead zirconate titanate) thick films deposited on silicon substrates can be used to bend the micro channels to vary the focal length of the MOAs. Thick-film PZT is more robust and easier to pattern than bulk PZT so it is chosen to provide actuation for the MOAs. In this project the manufacturing processes of thick-film PZT on silicon substrates are investigated, including ball-milling of starting powders, paste composition, paste preparation, doctor blading method, sintering regime, and poling. The particle size and surface area of the starting powders were measured to see the effect of wet ball-milling. Active thick-film PZT samples on silicon substrates have been successfully made. The thick-film samples were characterised using d_{33} measurement, impedance analysis, SEM, and XRD techniques. An average d_{33} of 76 pC/N has been achieved. A feasible method to manufacture thick-film PZT on silicon substrates has been summarised.

Keywords: PZT, thick-film, silicon substrate, doctor blading, piezoelectric material, ball milling, micro-structured optical arrays.

Acknowledgements

I would like to thank my supervisor Professor Tim Button and the technical staff member in my research group Mr. Carl Meggs for their support to my project. I would also like to thank my parents for their support and encouragement to me during my studies.

Table of Contents

List of Illustrations

List of Tables

Chapter 1 INTRODUCTION

Micro-structured optical arrays (MOAs) are micro channels etched in silicon substrates and can be used as mirrors to reflect and focus X-rays [1]. In order to vary the focal length of the focused X-rays, the silicon substrate needs to be bent and thus the MOAs are bent. Piezoelectric PZT (lead zirconate titanate) thick films deposited on silicon substrates can be used to bend the channels because PZT will produce strain when applied with a voltage. Thick-film PZT is more robust and easier to pattern than bulk PZT so it is chosen to provide actuation for the MOAs. In this project the manufacturing processes of thick-film PZT on silicon substrate are investigated. Thick-film PZT samples on alumina substrate have also been fabricated to make comparison.

In this thesis, Chapter 2 presents the literature review. It reviews the physics of piezoelectric actuators and thick-film piezoceramics. Following the literature review, the project objectives are outlined in Chapter 3. The experimental techniques used in this project are presented in Chapter 4, and the results and discussion in Chapter 5. Finally, the conclusions of this work and suggestions for further work are outlined in Chapter 6.

Chapter 2 LITERATURE REVIEW

2.1 The physics of piezoelectric actuators

When a piezoelectric material is applied with stress, it will generate electric charges on its faces. This is called the direct piezoelectric effect. Conversely, when a piezoelectric material is subjected to electric fields, it will experience strain, which is referred to as the inverse piezoelectric effect.

2.1.1 The crystallographic structure of Perovskite Electroceramics

Whether a material exhibits piezoelectric behaviour depends on whether there is net polarization in its unit cells [2]. Therefore, materials with cubic symmetry do not exhibit piezoelectricity. Perovskite-derived materials with a tetragonal structure are piezoelectric because the atom at the centre of the unit cell is slightly off-centre, which causes a net polarization in the unit cell. Applied pressure causes displacement of atoms within the unit cell and thus changes the electric dipole moment (direct piezoelectric effect). On the contrary, applied electric fields have forces on the electric dipole moment and then change the positions of the atoms (indirect piezoelectric effect).

$BaTiO_3$ is the prototype perovskite piezoelectric ceramic [2], so it is taken as an example to illustrate the perovskite structure. A cubic unit cell of $BaTiO_3$ is shown in Figure 2.1. There is a Barium atom at each corner of the cube. There is an Oxygen atom at the centre of each face of the cube. There is a Titanium atom at the centre of the cube. Above its Curie point (approximately 130 ℃) the unit cell of $BaTiO_3$ is cubic. Below the Curie point, the unit cell is slightly deformed to the tetragonal form with a dipole moment along the c direction. Below 0 ℃

the structure is orthorhombic with the polar axis parallel to a face diagonal. Below -90 ℃ the unit cell is rhombohedral with the polar axis along a body diagonal. The distortions are shown in Figure 2.2.

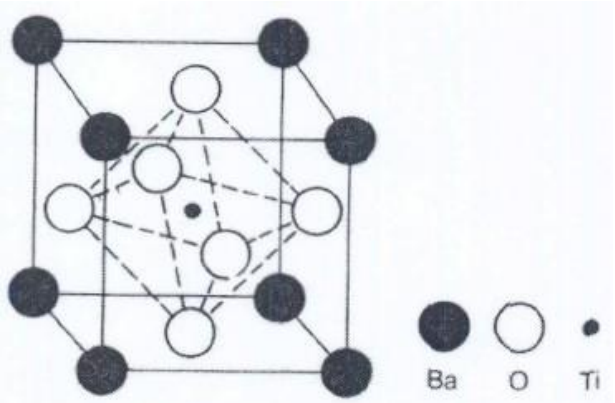

Figure 2.1: The unit cell of $BaTiO_3$. (after A.J. Moulson and J.M. Herbert[2])

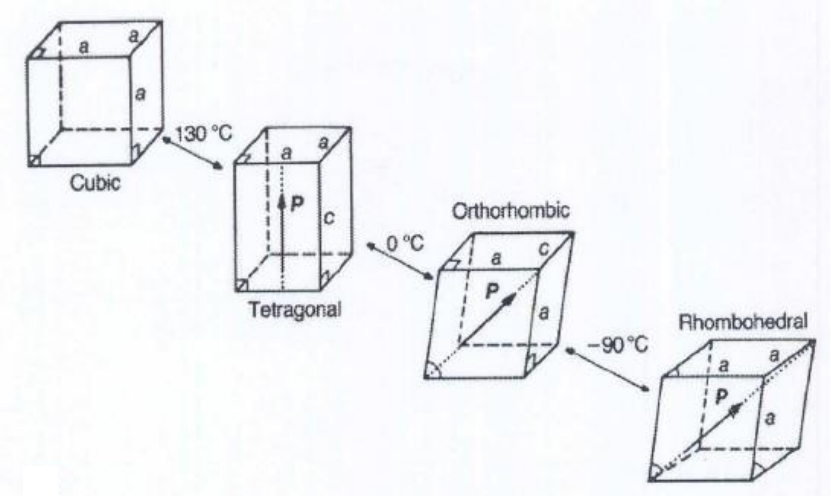

Figure 2.2: unit-cell distortions of $BaTiO_3$ (after A.J. Moulson and J.M. Herbert[2])

2.1.2 Piezoelectric domains

In real piezoelectric materials polarization is not uniformly distributed, but arranged in different regions referred to as domains. In each domain the polarization direction is the same. The net polarization of a material is the combination of polarization of all the domains. W.J. Merz studied domain formation and domain wall motions in $BaTiO_3$ single crystal [3]. When the electric field initially applied along the polar direction of single-crystal $BaTiO_3$ is reversed, new domains with opposite polarisation are formed. The polarisation is changed by formation

of very many new anti-parallel domains. These new domains grow only in the direction of the electric field. The speed of domain switching depends on applied electric field, temperature and the size of the sample.

2.1.3 The PZT phase diagram

Figure 2.3 shows the phase diagram of PZT [4]. The Curie point is the temperature at which the crystallographic structure of piezoelectric materials changes from tetragonal or rhombohedral to cubic structure. For PZT the Curie temperature changes when the relative concentrations of Zr and Ti change and when the concentration of dopants is changed. The material loses ferroelectric behaviour and becomes paraelectric above the Curie temperature because only the cubic phase is present.

In the PZT phase diagram the morphotropic phase boundary (MPB) is a significant feature[2]. At MPB the crystal structure changes abruptly with composition at constant temperature in a solid solution range. In the PZT phase diagram, the MPB occurs close to the composition where $PbZrO_3$: $PbTiO_3$ is 1:1. At MPB the tetragonal and rhombohedral phases coexist. There are six equivalent polarisation directions allowed in the tetragonal structure and eight in the rhombohedral structure. Therefore a PZT at MPB has 14 polarisation directions and thus has the best piezoelectric properties. This feature is exploited in commercial compositions.

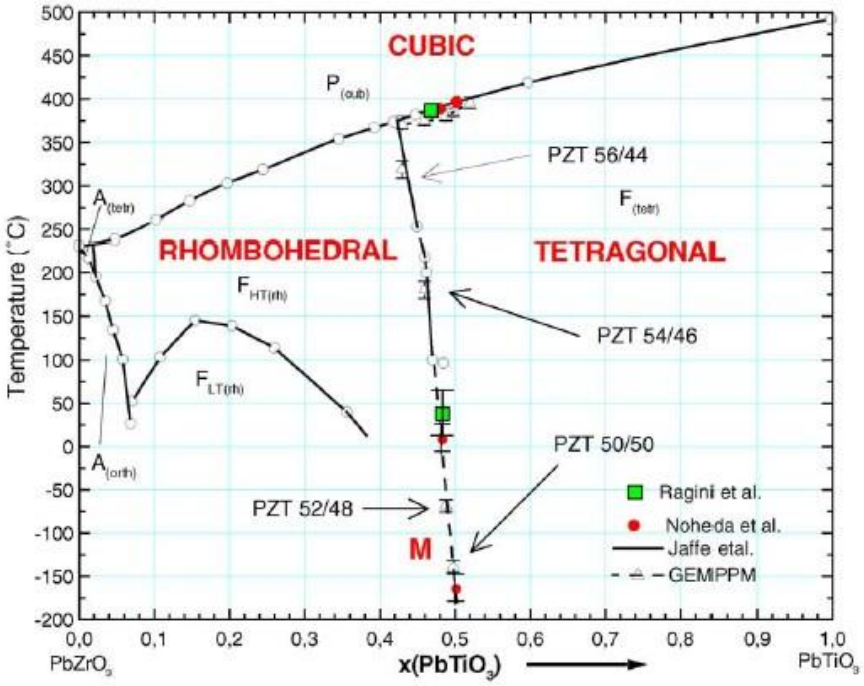

Figure 2.3 Phase diagram of Lead Zirconate Titanate (after Bouzid et al.[4])

2.1.4 Sintering

Sintering is an essential step in the manufacturing of piezoelectric ceramic. In the sintering process small particles of the material are bonded together by solid-state diffusion[2]. In sintered ceramic, crystallites are joined to one another by grain boundaries. The driving force for sintering is reduction of surface energy of the particles. After sintering, the high surface energy of the original small particles will be replaced by the lower energy of grain boundary surfaces of the sintered ceramic. Finer particles have higher surface area and thus higher surface energy. Therefore, finer particles are easier to be sintered than large particles. In the sintering process, the matter of neighbouring particles must diffuse into each other and the time taken to finish this process is proportional to the square of the particle size. The process will be significantly slower if the particles comprise aggregates of crystals rather than individual crystals. Aggregates usually densify more quickly internally than with

neighbouring aggregates, resulting in residue of pores in the spaces originally between the aggregates.

2.1.5 Poling of piezoelectric ceramics

Polycrystalline materials can also exhibit piezoelectric properties. In these materials, as the crystallographic orientation and thus polarization direction of their grains are random the net polarization is zero on average. To make a polycrystalline exhibit net polarisation, it has to be subjected to a poling process [1].

During the poling process, the piezoelectric material is heated to a temperature which is below, but close to the material's Curie temperature [1]. High temperature injects thermal energy into the material and increases the mobility of the domain walls. This condition is maintained for 10-20 minutes. In this period a high electric field is applied to the material. The external field causes the domains with polarisation approximately parallel to the field to grow at the expense of other domains. After the poling process, the material is cooled down to room temperature and the electric field is removed. At this time, the polarisation of all of the domains is approximately parallel to the poling electric field.

2.1.6 Linear and Non-linear Piezoelectricity

The defining equation of the piezoelectric charge constant d is as follows:

$$d = \left(\frac{\partial D}{\partial X}\right)_{E,T} = \left(\frac{\partial x}{\partial E}\right)_{X,T} \tag{2.1}$$

D is dielectric displacement, X is stress, E is electric field, T is temperature, and x is strain. The subscripts denote the parameters held constant. d represents the amount of charge

generated when unit stress is applied to the material, or the magnitude of strain produced when unit electric field is applied to the material.

In order to denote piezoelectric coefficients clearly, the convention is to define the poling direction as axis 3, as illustrated in Figure 2.4 [2]. Axes 1 and 2 are perpendicular to axis 3. The shear planes are indicated by the subscripts 4, 5, and 6 and are perpendicular to directions 1, 2, and 3 respectively. For example, d_{31} is the coefficient relating the field along the polar axis to the strain perpendicular to it, whilst d_{33} is the corresponding coefficient for both field and strain along the polar axis.

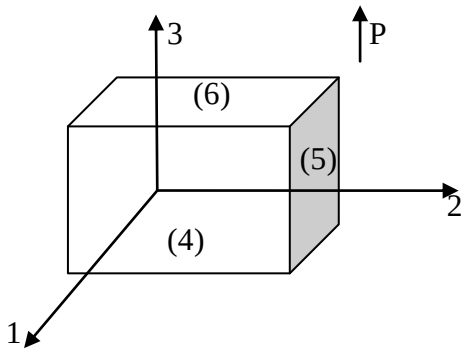

Figure 2.4 Labelling of reference axes and planes for piezoelectric ceramics.

When small electric fields or external pressure are applied to piezoelectric ceramics their piezoelectric behaviours are approximately linear. If the coefficient d is assumed to be constant, the direct and indirect effects can be expressed as

$$D = dX + \varepsilon^X E \tag{2.2}$$

and

$$x = s^E X + dE \tag{2.3}$$

respectively [2], in which s is the elastic compliance of the material, and ε is the dielectric constant of the material. The superscripts denote the parameters held constant.

When piezoelectric ceramics are applied with high electric fields, their piezoelectric behaviours become non-linear and there are hysteresis effects.

2.1.7 Characterisation

The piezoelectric charge constant d_{33} is often used as a defining piezoelectric characteristic for improvement of piezoceramic technology. The most commonly used method to measure d_{33} is the so-called direct or Berlincourt method in which a force is applied to piezoceramic and the generated electric charge is measured. In the thick-film technology the piezo-layers must be printed on substrates. Therefore, one must take care when measuring thick-film samples because substrates can bend during measurement and lead to inaccurate readings. By changing the substrate supporting structure, a Berlincourt method based piezometer can also be used to measure e_{31} [5]. The sample is supported by a ring structure, and the upper force is applied on the surface of the sample at the centre of the ring. Some basic mathematical treatment is involved in the analysis which is presented in [5].

Dorey and Whatmore [6] investigated the influence of substrate clamping on measured d_{33} in their study on sol-gel thick-films. The substrate clamping effect produces stresses in PZT films which deform the unit cells and reduce the effectiveness of the poling process.

Torah et al.[7] think that the clamping effect reduces the measured piezoelectric coefficient of the film. The reduction is due to the influence of d_{31} component in the film. Theoretical analysis predicts that d_{33} reduces by 62%. This result was obtained with Equation (2.4) and properties of standard PZT-5H bulk material and 96% pure alumina substrate. In this equation, d_{33} and d_{31} are piezoelectric charge constants of standard bulk PZT-5H material. $d_{33,f}$ is the effective d_{33} of the film. D_3 and T_3 are electric displacement and stress along axis 3 respectively. s_{11}, s_{12}, s_{13} are compliances of bulk PZT-5H. ν_{sub} and Y_{sub} are Poisson's ratio and

Young's modulus of the alumina substrate respectively. The complete analysis of Equation (2.4) is presented in [7].

$$\left(\frac{D_3}{T_3}\right)_E = d_{33,f} = d_{33} + 2d_{31}\left(\frac{-\left(\frac{v_{sub}}{Y_{sub}}\right) - s_{13}^{E}}{s^{E}_{11} + s^{E}_{12}}\right) \tag{2.4}$$

The measured clamped d_{33} of PZT-5H thick-films from that study is 130 pC/N, which is equivalent to an unconstrained value of 350 pC/N.

It is significant to recognize the clamping effect when citing measured piezoelectric properties. Therefore, the piezoelectric coefficient of thick films is denoted as $d_{33,f}$ to signify that it is a film rather than a bulk piezoceramic. A summary of thick-film PZT data from the literature is presented in Table 2.1.

Table 2.1: a summary of thick-film PZT data from the literature

No.	PZT type	substrate	details	$d_{33,f}/pCN^{-1}$	Reference
1	PZT 5H	96% alumina substrate	A blend of ball and attritor milled PZT powders with a lead borosilicate binder was used. Films were fired at 1000℃. Other details are not mentioned in the reference.	131	[7]
2	PZT 5H	96% alumina substrate	10 wt% of Ferro 7575 lead borosilicate glass powder was added to the PZT powder. The powders were then wet ball milled with milling media. 5～8ml of vehicle (ESL 400) was used in each batch to mix the powders to form a paste. The paste was then mixed using a triple roll mill. Then the paste was screen printed and dried at 140℃. Films were fired for 34 min (peak temperature 890℃) and poled with a field of 4 MV/m at 150℃ for 30 min.	52±3.2	[8]
3	PZT 5H	silicon	The PZT paste was made from 95% PZT-5H powder and 5% lead borosilicate glass powder and 5ml ESL 400 organic vehicle. The paste was mixed using a triple roll mill. Then it was screen printed and dried at 140 ℃.The samples were fired at 800℃ for 8h and then poled at 150℃ in a field of 3 MV/m for 40 min.	109±2.9	[9]
4	PZT 5H	silicon	Fired at 850℃ for 8h. The other details are the same as No. 3.	102±3.5	
5	PZT 5H	silicon	Fired at 950℃ for 1h. The other details are the same as No.3.	127±16.1	
6	PZT 5H	silicon	Fired at 1000℃ for 1h. The other details are the same as No.3.	169±5.6	
7	PZT 501A Ultrasonic Powders Inc.	silicon	4 wt% Li_2CO_3 and Bi_2O_3 (at equimolar concentrations) glass was mixed with PZT powder in a vibratory mill for 24h. The paste was made from 69% PZT powder, 22% DuPont organic vehicle and 9% α-terpineol solvent. The paste was mixed using a three roll mill. Then it was screen printed and dried at 110℃ for 1h. The sample was fired at 850℃ for 15 min.	50	[10]

2.2 Thick-film piezoceramics

2.2.1 Introduction and History

The development in the area of microelectronics has largely driven the advance of micro-sensor technology [11]. Currently silicon planar technology is widely used in fabrication of

many sensors. But its drawback restricts its ability to provide an economic solution to low-to-medium-volume demands (e.g. a few tens of thousands of sensors per year).

The thick-film technology was introduced as a method of fabricating hybrid circuits about 46 years ago. These hybrid circuits consist of semiconductor devices, monolithic ICs, other discrete devices and thick films themselves. These hybrid circuits made using thick-film technology have the advantage of being compact, robust and relatively inexpensive. They are applied in areas such as televisions, telephones, calculators, automotive electronics and so on. In the past 25 years or so, thick-film technology has also been successfully used to make powerful and cost-effective sensors.

Piezoelectric thick-films were firstly described by Baudry in 1987 [12]. He manufactured an acoustic coupler to show an application of the technology. The thick-film material was based on the mixture of lead zirconate titanate (PZT) powder, a small amount of glass frit, and an organic vehicle.

The piezoelectric charge constant d_{33} is an important parameter for sensor and actuator applications [13]. It is an indication of the sensitivity of the film because it relates electric charge produced with a given applied mechanical stress. This property is particularly important in planar film technology because the electrodes of these films are on the upper and lower surfaces of the films and thus the direction of the poling field and measurement are both in the '3' axis. For bending applications, the piezoelectric coefficient d_{31} is also important.

There are many various piezoelectric materials, such as Quartz, Barium Titanate, Lithium Niobate, and Lead Zirconate Titanate. However, the most commonly used piezoelectric material is Lead Zirconate Titanate (PZT) because it has the best piezoelectric properties.

2.2.2 Formulation

A PZT thick-film generally begins as a thixotropic paste which is able to pass through a screen easily but retain subsequent printed shapes [13]. The paste comprises active piezoelectric material, a suitable ceramic binding agent, such as lead borosilicate glass, and an organic vehicle, to ensure the paste is thixotropic and thus suitable for deposition. The percentages of the ingredients depend on specific application and process.

The study of Torah et al. emphasized the importance of the formulation of the paste to the piezoelectric properties of thick-films [8]. It was shown by studies that the milling process of PZT powders determines the homogeneity of the paste and thus the consistency of the printed thick-films. Ball, Attritor and Jet milling of PZT powder were investigated. The average particle sizes of powders produced by ball, attritor and jet milling were 2, 1.2 and 4.3 μm respectively. Ball milling produced smooth, circular particles in a reasonably tight particle size distribution. Attritor milling can further tighten the particle size distribution and can produce powder of a more uniform particle size. Jet milling is more abrasive than ball milling and produced powder particles in irregular shapes and a wider size distribution.

It was discovered that the larger particle size of the ball milled powders had the highest piezoelectric performance but that the tighter particle size distribution of the attritor milled powders had the most consistent results. Further work studied the combination of ball and attritor milled powders to optimise the films. The results showed the best paste formulation is 18% Attritor and 72% Ball milled PZT powders, with 10% lead borosilicate glass by weight.

2.2.3 Substrates

Unlike bulk materials, thick-film piezoceramics are deposited onto a substrate to provide support to the films when they are dried and sintered. The substrate is therefore an essential

part of the design and fabrication of thick-film devices. Below is the introduction of the two kinds of substrates used in this project.

2.2.3.1 Alumina substrates

Alumina substrates are used in many PZT thick-film devices because they are cheap and have good adhesion to the printed layers. Besides, the thermal expansion coefficient of alumina is closely matched to those of most PZT sintered films.

2.2.3.2 Silicon substrates

Thick-film sensors can be printed directly on to silicon substrates to be integrated with electronics on to the same chip. In addition, the size control attainable with micromaching and good mechanical properties of silicon increase the variety of thick-film PZT/MEMS applications including resonators, accelerometers and micro-pumps [14-16]. However, lead diffusion from the thick-film layers into the silicon substrate during sintering is an important problem for MEMS applications. Study by Maas et al. [17] has examined the use of a screen-printed barrier layer Heraeus IP211 to prevent lead diffusion. An alternative to the barrier layer is to reduce the sintering temperature as there is less lead diffusion at lower temperature. But the lower sintering temperature can cause porosity and thus poor sintering of the films.

2.2.4 Fabrication

Thick-films are deposited using a doctor-blading or a screen-printing process. Screen-printing is an attractive process in MEMS applications because it allows to batch print various patterns on different substrate materials. The process is suitable for mass production and can be used to fabricate films of thickness 10-100μm in a single print stroke. In preliminary studies, a doctor-blading process can be used to investigate the suitability of thick-films for specific applications, as it is simpler than screen printing.

2.2.4.1 Screen-printing process

The four steps of the screen-printing process are shown in Figure 2.5 [13]. (a) The paste is spread across the screen with a flood blade and is ready for printing. (b) Then a print stroke starts. A squeegee forces the screen down on to the substrate. (c) The squeegee is moved across the screen. It forces the paste through the etched parts of the mask and removes the redundant paste. (d) Finally, the pressure of the squeegee is removed. The screen returns to its initial position and leaves the paste deposited on the substrate in the desired pattern. The print stroke ends.

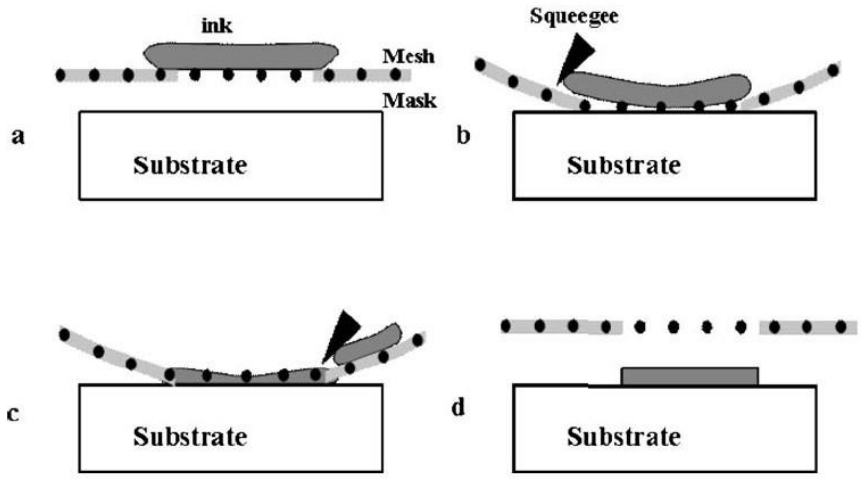

Figure 2.5: Process steps for screen-printing (after R.N. Torah et al.[13])

The screen printing process allows many layers to be printed in sequence. The printed layers are dried before the next layer is printed. The thickness of the printed layer is controlled by the printing pressure and the gap between the screen and the substrate. Therefore, as the number of printed layers increases, it is necessary to enlarge the gap size to make sure the screen can spring back without smearing the print.

2.2.4.2 Doctor blading process

The doctor blading process was used by A. J. M. Frood et al. to fabricate thick-film piezoelectric elements on silicon[18]. They firstly formed patterned features using photoresist on silicon wafers, then doctor bladed piezoelectric paste using a rubber squeegee across the wafers to fill the paste in the features. After drying PZT, the shrinkage leaves space to doctor blade top electrode. After drying top electrode, they removed the photoresist and fired the PZT. A schematic diagram of the process is shown in Figure 2.6. This technology achieved better alignment accuracy and resolution than the screen printing process.

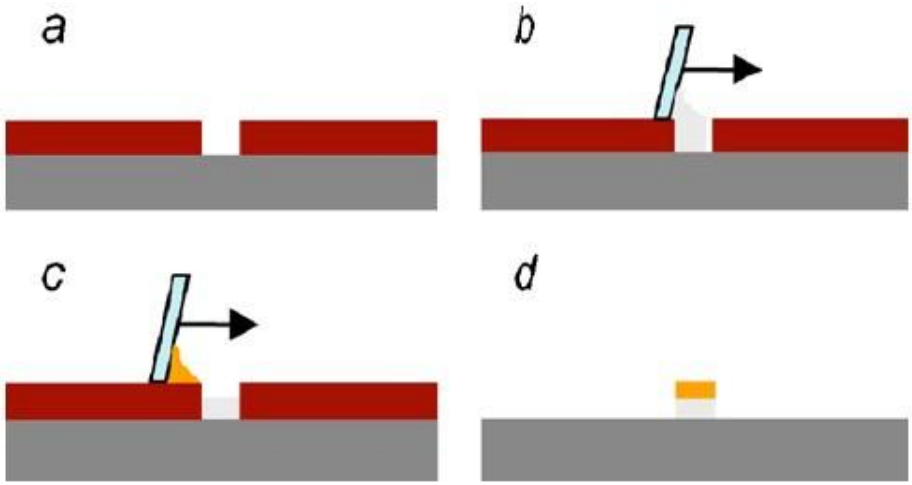

Figure 2.6: A schematic diagram of the doctor blading process. (a) photoresist with patterned features on silicon wafers. (b) Doctor blade PZT paste across the wafer to fill in the features. (c) Dry PZT. Shrinkage leaves space to doctor blade top electrode. (d) Dry electrode, remove the photoresist then sinter.

2.2.4.3 Firing process

Dried films of the piezoelectric ceramic with glass addition should be sintered at a suitable temperature (generally about 900℃) to melt the binding material (a lead-based glass) and form a bonding matrix for PZT powder. The films are composite material which has different electro-mechanical properties from those of bulk material.

Glynne-Jones et al. have studied the firing profile for thick-film layers on silicon [9]. The films were based on PZT type 5H supplied by Morgan Electro Ceramics Ltd., and were sintered over a range of temperature from 750 to 1000℃. It was found that films fired at the lower temperature of 750℃ showed poor sintering. Films sintered at temperatures above 800℃ showed acceptable adhesion and density. The films sintered at the lower temperature showed d_{33} values of between 101 and 109 pC/N. The samples sintered at 1000℃ had the highest value of 169 pC/N. This is because of the improved sintering of the film at the higher temperature. However, the higher temperature has a disadvantage that it causes lead to diffuse from the PZT to the silicon and pollute the surface of the silicon.

2.2.5 Thick-film piezoceramics on silicon substrates

Thick-film PZT is more robust than bulk PZT [13], particularly important in the application being considered here. Screen printing can deposit PZT in the desired patterns without the need for subsequent photolithographic or etching steps.

There are some disadvantages of thick-film technology [13]. Micromachined silicon wafers are too fragile to withstand the pressure inserted by screen printing process. The resolution and alignment accuracy of screen printing is worse than those of photolithography. Some researchers tried to deposit PZT thick-film and electrodes layers on silicon firstly and then perform standard micromachining such as photolithographic and wet and dry etching processes. They have successfully made some devices. But the lead migration reaction products were found to inhibit the subsequent etching processes and cause difficulties in accurately defining structures. Thiele et al. have investigated the reaction process and reported that the reaction product is a lead silicate [19].

Frood et al. developed a doctor blading process to improve resolution and alignment accuracy [18]. They used thick photoresist to form patterns on platinised silicon and then doctor bladed PZT and gold electrode to fill in the features. After removal of the photoresist, the PZT was fired. The resolution and alignment accuracy achieved with this process is comparable with standard photolithographic processes (minimum feature sizes<50 μm, a film thickness of 100 μm). A d_{33} value of 60 pCN^{-1} was measured with piezoelectric elements successfully poled on a silicon wafer.

2.2.6 Devices

Thick-film piezoelectric devices have been fabricated for various applications. The following are some examples.

2.2.6.1 A thermally compensated thick-film accelerometer

Several different structures of piezoelectric thick-film accelerometers have been reported. Crescini et al. have developed a thermally compensated thick-film accelerometer[20]. One sensing element was screen printed on either side of the alumina substrate in a planar capacitor structure for the purpose of reducing thermal drift. The alumina substrate was 635 μm thick and 6 mm in diameter. Each of the sensing elements consists of a PZT layer (40－50 μm thick) sandwiched by two conductive layers based on Pt/Au material. The PZT was poled under an electric field of 3 MV/m for 15 min at 180 ℃ and obtained a d_{33} of 180 pC/N. When an acceleration is applied to the device, one PZT layer will be compressed and the other will be extended due to the intrinsic mass of the device. The strain of the PZT layers will generate charge on their electrodes so the acceleration can be sensed. To cancel out the effect of thermal drift on the device, the two PZT films were connected in series. The two units were poled in the same axis but opposite directions. As a result, thermal drift in one unit will be

opposite to that of the other unit and the effect is therefore cancelled out. Figure 2.7 shows a schematic of the device.

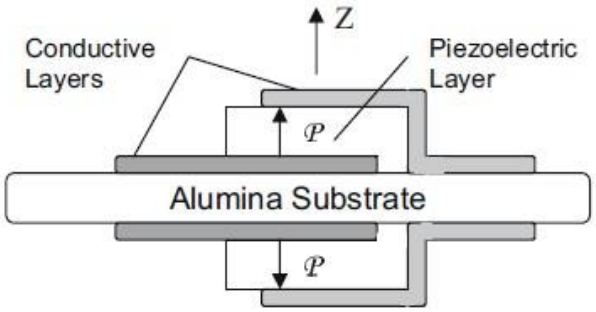

Figure 2.7 Cross-sectional view of the cylindrical structure of a thick-film accelerometer (after Crescini et al.[20])

2.2.6.2 A thick-film PZT/micromachined silicon accelerometer

Another example of a combined thick-film and silicon micromachined device is the accelerometer reported by Beeby et al.[21]. This accelerometer had a 17 mg inertial mass suspended by four silicon beams. Each of the silicon beams was located at a corner of the inertial mass. On each of the beams a piezoelectric sensing unit was screen printed. Each sensing unit was a planar capacitor structure with the active PZT layer sandwiched between top and bottom electrodes. The silicon structure was fabricated by silicon micromachining method as presented in [21]. When an acceleration is applied to the inertial mass it will move relative to the chip frame and therefore will cause the supporting beams to deflect. The piezoelectric layers on the beams will deform as well and thus generate charges. In this way the acceleration is transformed into electrical charges and can be sensed. The amount of charges induced depends on the piezoelectric properties of the sensing material and is proportional to the deflection of the beams. Figure 2.8 illustrates a finite element model of the device, and a scanning electron micrograph of the actual device.

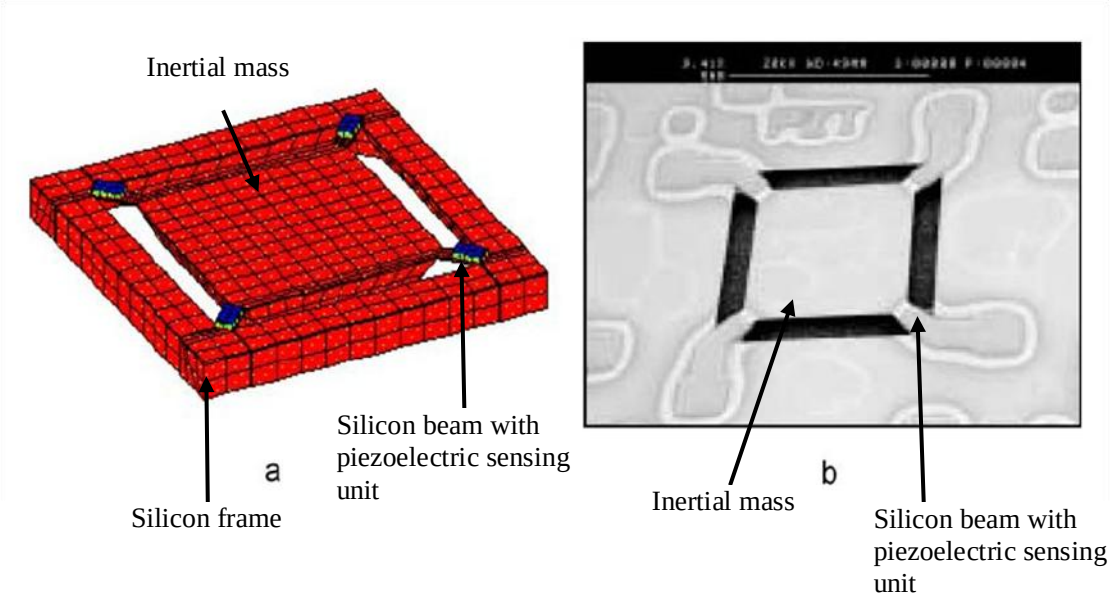

Figure 2.8 a) Finite element model and b) scanning electron micrograph of a combined thick-film/silicon accelerometer (after Beeby et al.[21])

The bottom electrodes of the sensing elements was a 500 nm thick platinum layer with a 50nm thick titanium layer which were electron beam evaporated onto the silicon wafer. The PZT paste used was made from 95% PZT-5H powder, 5% lead borosilicate powder and 5ml ESL 400 organic vehicle. Each PZT layer was printed by two print strokes and had a thickness of the order of 60 μm after drying and sintering. The PZT was fired at 890 ℃ for 1h. Then a gold cermet ink was printed onto the PZT to form the top electrodes with a thickness of about 10 μm and fired with the same sintering regime as used for the PZT. Then the PZT was poled at 150 ℃ for 1h under 400 V (equivalent to a field strength of 6.67 MV/m). Test results showed that the sensitivity of this accelerometer was 16 pC/g, which was more than 100 times greater than the sensitivity (0.15 pC/g) of a piezoelectric ZnO thin-film silicon accerlerometer [22].

2.2.6.3 Micropump

The micropump is another example of combining screen-printed PZT thick films with micromachined silicon structures. Koch et al. [23] described a micropump consisting of three silicon wafers which were fusion bonded together. The device is shown in Figure 2.9.

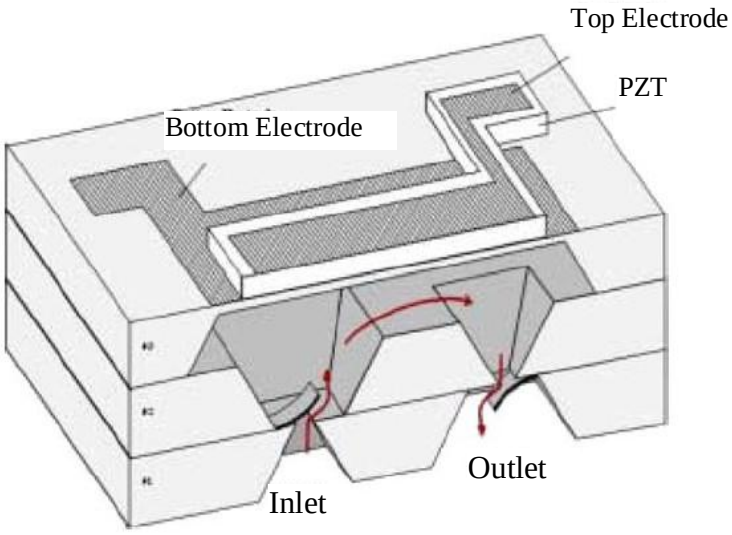

Figure 2.9 Combined silicon/thick-film micropump (after Koch et al.[23])

The passive cantilever valves were manufactured using a boron etch stop technique and fusion bonding. Tests of the valves exhibited satisfying performance, since no flow could be detected in the opposite direction. Initial experiments on a thick-film screen-printed piezoelectric membrane actuator were conducted. An exploration of suitable pastes for electrodes on various insulation layers on silicon discovered silicon dioxide and cermet gold paste as the best combination. The printed PZT ink consisted of 19.5g PZT-5H powder, 0.5g borosilicate powder and 5 ml organic vehicle (ESL 400). The bottom electrode was printed twice, dried at 120 ℃ for 10 min and sintered at 950 ℃ for 1h. Then the PZT layer was printed with two printing twice, drying and sintering cycles at the above conditions to obtain a thickness of 100 μm. Finally, the top electrode was printed on PZT at the same conditions as for the bottom electrode. Both the top and bottom electrodes were based on cermet gold inks. The PZT film

was then poled in a field of 3 MV/m for 30 min at 120 ℃. After poling, the PZT showed a d_{33} of 95 pC/N.

Deflection measurements showed that a 7×3 mm PZT and 8×4 mm silicon bimorph membrane produced 1 μm movement at an applied voltage of 100V. A quasi-static simulation package of the flow through the micro pump was also conducted. The valve action was simulated with the ANSYS finite element package and FLOW3D. Pump rates of up to 400 μl/min with a maximum backpressure of 35 kPa were achieved when 100 V driving voltage was applied across the PZT. Lead pollution around the area of PZT was found and this caused the SiO_2 insulation layer to become conductive.

2.2.6.4 Development of spider actuators for the MOAs

In this thesis the Micro-structured Optical Arrays (MOAs) application is what the thick-film PZT actuators are used for. This subsection describes the development of the MOAs.

2.2.6.4.1 Introduction

The MOA concept is mainly based on polycapillary [24] and microchannel plate optics [25], in which X-rays are reflected multiple times by a large number of small channels. A schematic of an MOA is shown in Figure 2.10, where X-rays from a point source (at the top of the figure) are guided to a (quasi-) point focus at the bottom by two successive reflections. The first MOA is curved. By adjusting its radius of curvature the focal length can be adjusted [26]. The second MOA is flat. The channels of the two MOAs can reflect X-rays because their walls are very smooth (roughness<2 nm [1]). There is a central block (not shown in the figure) in the first array stopping un-reflected X-rays from reaching the focus. Many more channels would be used in practice. The required Radius of Curvature (ROC) for the curved MOA is 5 cm.

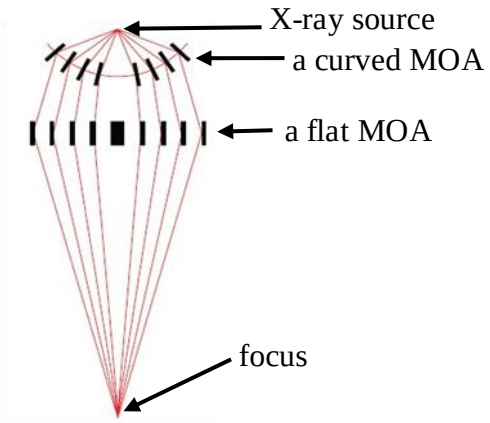

Figure 2.10: Operation principle of a curved/flat tandem MOA configuration. Incident X-rays from a line source (top) are guided to a line focus (bottom). (after Michette et al.[27])

2.2.6.4.2 Manufacture of MOA channels

Manufacture of the MOAs have been investigated as part of the Smart X-ray Optics project carried out by a UK based consortium comprising researchers from the following institutions: the Mullard Space Science Laboratory, University College London, Kings College London, the University of Leicester, the University of Edinburgh, the University of Birmingham and the Science and Technologies Facilities Council Daresbury Laboratory [28].

The MOA channels were manufactured on silicon substrates using both dry-etching and wet-etching techniques [29, 30]. MOA channels with an 18:1 aspect ratio were manufactured and similar channels with 32:1 aspect ratio have been achieved (see Figure 2.11). The surfaces of channels manufactured using dry-etching technique had regular patterns (scalloping), which increase the surface roughness (see Figure 2.12). The sidewall roughness was of the order of 10 nm, which is beyond the requirement of 2 nm. Therefore, the wet etching technique was used to manufacture the channels. Using this method channels with sidewall roughness of 1.2 nm were successfully fabricated. Thus the sidewall roughness requirement was satisfied.

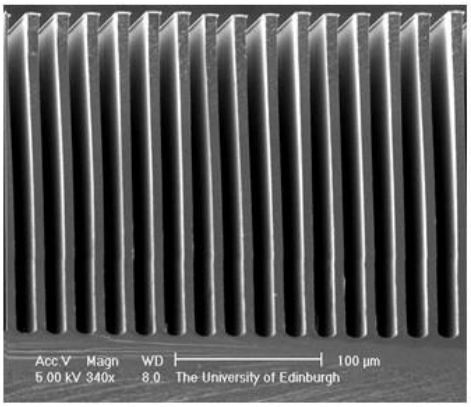

Figure 2.11 SEM picture of MOA channels manufactured using a dry-etching technique on silicon substrates. The channels are 20 µm pitch etched into silicon with an aspect ratio of 18:1 (similar channels with 32:1 have been achieved). The wafer was not fully etched to allow cleaving for inspection by SEM. (After Alan Michette et al.[30])

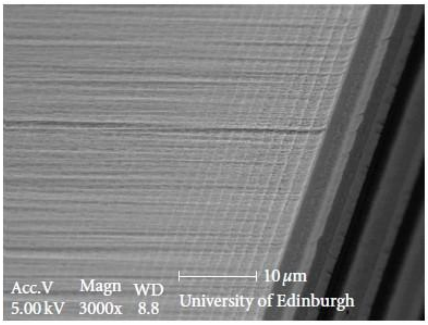

Figure 2.12 SEM picture of the regular patterns (scalloping) on the sidewalls of the MOA channels. (after Alan Michette et al.[26])

2.2.6.4.3 The initial actuator design for the bending of the MOAs

An initial design of actuators for MOA chips was proposed [1], where the MOA channels are etched in the central 2 mm × 2 mm area of a silicon wafer (2 cm × 1 cm × 100 µm). The actuation is provided by two PZT strips (2 cm × 2 mm × 60 µm) bonded along each side of the length of the wafer. The design is illustrated in Figure 2.13.

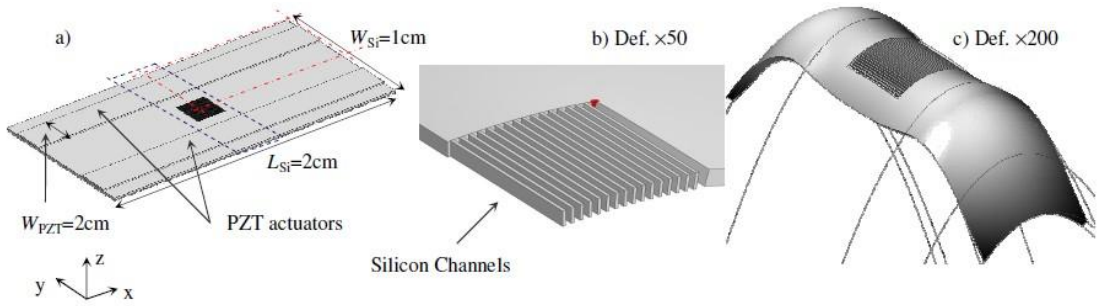

Figure 2.13: a) Initial model of the MOA chip. b) An enlarged view of a quarter of MOA channels. c) Exaggerated deformation of the model. (After Rodriguez-Sanmartin [31])

This design was simulated using a finite element analysis (FEA) model. In simulation a voltage of 120 V was applied to the PZT strips. Figure 2.13(c) shows the 3D deformation of the MOA chip. The deformation has been exaggerated for visualization purposes. The radius of curvature of the MOA channels in the FEA model is 28 cm. This value is more than five times larger than the required 5 cm target.

A prototype device of the initial actuator design was fabricated and tested. The test results showed that the device had a maximum ROC of 42 cm. Therefore, both the FEA analysis and the prototype device demonstrated that the initial design would not be capable of producing the required ROC. Therefore a better design was needed.

The viscous plastic processing (VPP) technique [1] was used to produce thin sheets (~100 μm thick) of green piezoelectric material. Then layers of platinum ink (~20 μm thick) were screen printed on both sides of the green sheets. Then the sheets were cut into small pieces. After that, they were sintered buried in lead oxide sand in a crucible to maintain the lead stoichiometry of the samples. After sintering the samples were poled in an oil bath. The poling was performed for 5 minutes at 190℃ and 150 V.

2.2.6.4.4 The initial spider MOA design

As the initial actuator design was shown not to generate sufficient curvature for the MOA structure, a new configuration was devised [1]. In this configuration, several levers were formed by etching angled channels through the silicon chip. These levers connected the two edges of the silicon chip with its central area. Two PZT strips were bonded along the two edges respectively. The levers transfer the actuation from the edges to the centre and amplify it in the process. The pattern of the levers was like a spider so this design was called a 'spider' design.

2D modelling was performed to determine the optimum thickness ratio of PZT and silicon for obtaining the maximum bending. Modelling results showed that the maximum bending could be obtained with the ratio T_{PZT}/T_{Si}~0.6 [31]. Then FEA models of the spider MOA design were established as shown in Figure 2.14 [32]. In these models the thickness of the PZT strips and silicon chip were 60 μm and 100 μm respectively, in accordance with the optimum ratio of 0.6. The piezoelectric coefficients chosen were those of PZT-5H ceramic (d_{33}=593 pC/N, d_{31}=-274 pC/N). The thickness of the bonding layer between the actuators and the silicon wafer was assumed to be zero. In the simulation a voltage of 150 V was applied to the piezoelectric actuators. The vertical displacement at the edge of the chip was 280 μm. The ROC in the centre 2 mm of the chip (across the channels) was 4.5 cm which satisfied the 5 cm target.

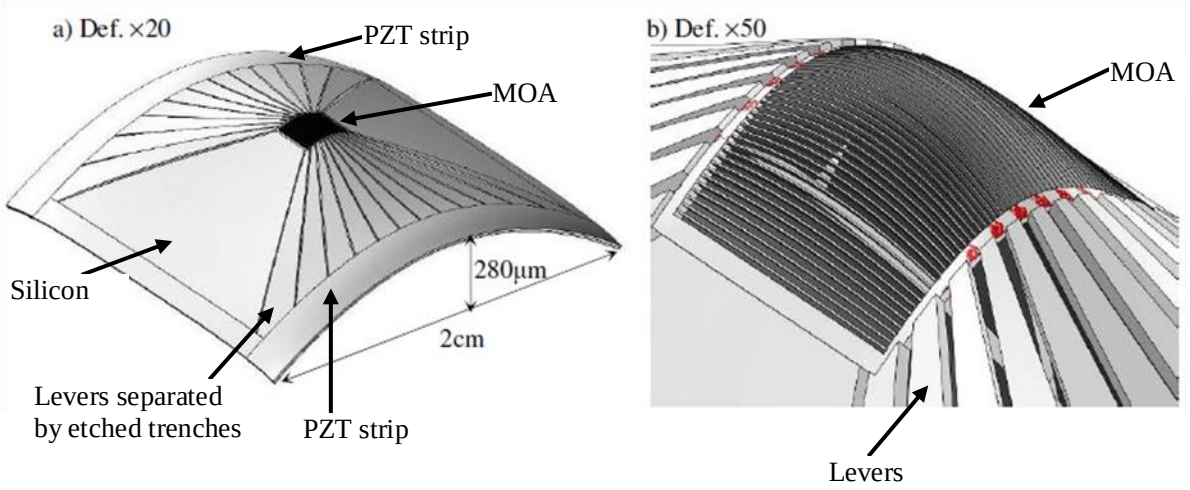

Figure 2.14: a)an FEA model of the initial spider MOA design. A voltage of 150 V was applied to the PZT actuators. b)exaggerated deformation (×50) of the central MOA channels [32].

Test spider structures were manufactured using a dry etching process [33]. Figure 2.15 shows a test device comprising a silicon wafer with spider patterns dry etched on it, and two piezoelectric actuators mounted on it. The characterisation results indicated that the device produced a ROC of 3 cm at its centre.

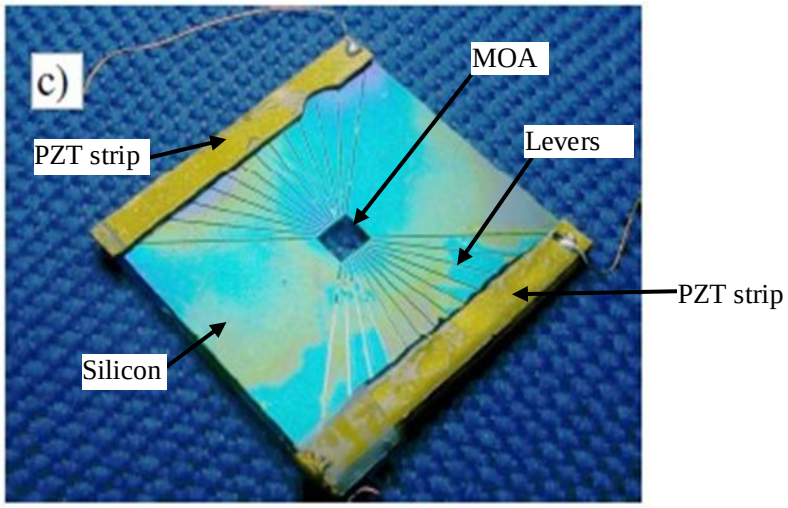

Figure 2.15: A dry etched spider MOA silicon chip (2 cm ×2 cm ×100 μm) with two PZT actuators (2 cm ×2 mm ×120 μm) mounted on it [32].

2.2.6.4.5 Wet etching compatible spider MOAs

The spider pattern was re-designed so that it could be wet-etched in the same manufacturing step as the MOA channels [32]. Figure 2.16 shows the redesigned spider pattern, in which the levers are drawn using two sets of planes. One set of planes are parallel to the silicon channels. The other set of planes are at an angle of 70.53 °coinciding with the second set of {111} planes on (110) silicon. Then the ROC of a test device was measured using a laser illumination method. The ROC of the channels was from 6.5 cm on the left to 5 cm on the right.

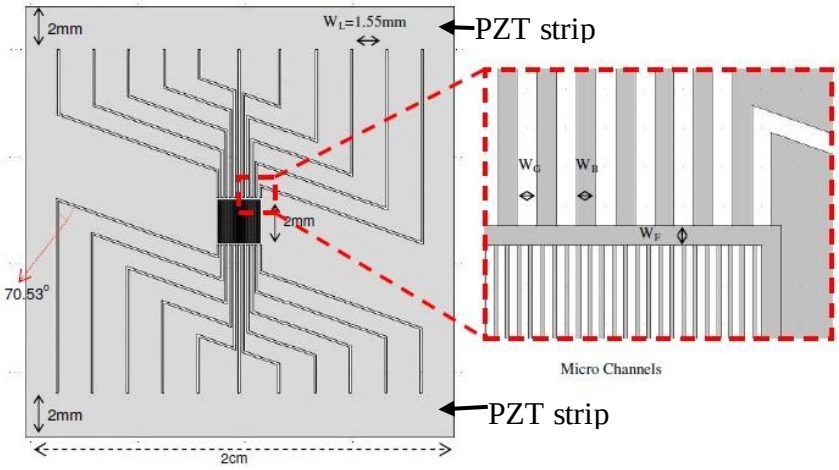

Figure 2.16: A schematic picture of the wet etching compatible spider MOA chip. PZT strips are bonded along the two outer 2 mm edges of the chip as labelled in the figure.(after Rodriguez-Sanmartin et al.[32])

2.2.6.4.6 Optimization of the actuator layout

The initial design of the piezoelectric actuators was just two piezo strips bonded to the outside 2 cm×2 mm edges of the silicon. Then this simple design was improved to add extra capabilities to the spider MOA chip [32]. In the optimised design, the piezoelectric actuators were extended to actuate more areas of the silicon. The electrodes of the piezoelectric actuators were divided into small segments so that different voltages could be applied to different segments of PZT. These improvements allow the profile of curvature of the MOA

channels to be controlled more flexibly. A schematic of the new design is shown in Figure 2.17. However, the segmented piezoelectric actuators have not been fabricated to date. This is because they are very fragile and easily broken when being manufactured and handled as 'stand alone' strips.

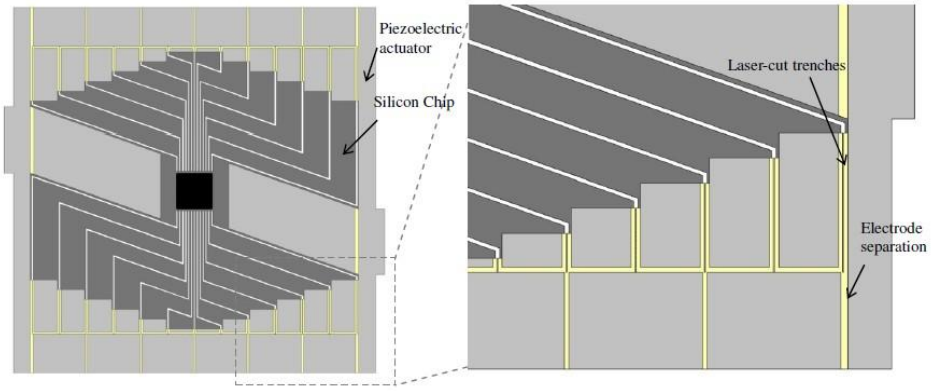

Figure 2.17: A schematic of the design of segmented PZT on a spider MOA chip (after Rodriguez-Sanmartin et al.[32])

Chapter 3 OBJECTIVES

The aim of this project is to investigate techniques for the integration of PZT actuators with silicon devices. The investigation will use thick film technology (doctor blading method) to deposit PZT on silicon test samples and then characterise the microstructure and functional properties of the samples, with particular emphasis on their suitability for the MOA application. These thick-film samples on silicon substrates will be compared to thick-film samples on alumina substrates, in order to investigate the influence of silicon substrates on the piezoelectric properties of PZT thick films.

Chapter 4 EXPERIMENTAL TECHNIQUES

4.1 Characterisation of the starting PZT powders

Particle size measurement was done with as-supplied PZT powders and wet ball-milled PZT powders (TRS 610C, batch 2002 and 2008, TRS Technologies, USA). This was performed using a particle sizer (Sympatec Limited) controlled by WINDOX software. The PZT powder was mixed with distilled water to form a suspension which was then poured into the chamber of the particle sizer. The stirrer and sonicator in the chamber were turned on to spread the powder particles homogeneously. Finally, data and graphics were obtained from the software.

Surface area measurement was also done with as-supplied PZT powder of both batches, and borosilicate glass powder. The instrument used was Micromeritics ASAP 2010.

4.2 Manufacture of thick film samples

4.2.1 Preparation of PZT ink and silver ink

A good way to prepare PZT ink has been found by investigation. 79.2 g PZT powder (TRS 610C) was mixed with 0.8 g borosilicate glass powder (Particle Technology, Foston, Derby's, UK) using a stirrer. Then zirconia milling media (in the size range 2～8 mm) and distilled water were added to the mixed powders. The weights of zirconia milling media, mixed powders and distilled water are in the proportion of 2:1:0.8. The mixture was put in a bottle and shaken manually for one minute to mix the components homogeneously. Then it was milled using a Ball milling machine (Machine No. 21735, Pascall Engineering) for 24 hours to break down agglomerates and reduce the measured PZT particle size for better sintering effect and thus better piezoelectric properties.

After that, the milling media was taken out of the bottle and washed using distilled water. The washing water was collected and added back to the bottle to recycle the PZT attached with the milling media. The paste in the bottle was poured into a glass beaker and dried in an oven at 80 ℃ until solid PZT was obtained. Then the solid PZT was ground into a fine powder using a mortar and pestle.

Then the powder was blended with 20 ml Blythe organic vehicle (Johnson Matthey, Stoke on Trent, UK). The mixture was put on a glass plate and a spatula was used to mix the powder and organic vehicle thoroughly to obtain a paste. Then the paste was processed by a three-roll mill (G2996-84/484/2 Marchant Engineers) three times to distribute the powder particles evenly in the paste and further break down the agglomerates. The roll gap sizes of the three-roll mill are 250 μm and 20 μm respectively. Finally, homogeneous PZT ink was obtained and collected in a bottle for subsequent use.

Silver ink was prepared using silver powder (Silver Flake FS2, Batch 114760, Johnson Matthey). 70 wt% silver powder and 30 wt% Blyth organic vehicle were blended and processed by the three-roll mill for three times.

4.2.2 Doctor blading method

In this project, doctor blading method was used to deposit thick films of materials (PZT, silver or platinum) on substrates (silicon or alumina). PZT and silver inks were produced using the method described in Section 4.2.1. The platinum ink used was a commercial ink (Gwent Electronic Materials Ltd) whose composition is kept secret by the manufacturer. In this method, four strips of PVC tapes (PVC Electrical Insulation tape BS 3924, thickness 130 μm) were applied onto a substrate to define a rectangular deposition area. Four strips of tapes formed the four edges of the rectangle. The thickness of the tapes controlled the thickness of

the deposited material. Then appropriate amount of ink was placed within the rectangular area. Then a plate with a flat edge was used to scrape the ink into a flat surface and fill the whole defined area with the ink. After that, the tapes were peeled off and only the rectangular ink area remained on the substrate. A schematic diagram of this process is shown in Figure 4.1. Finally the film was dried with the substrate in an oven (Lenton Thermal Designs) at 80 ℃.

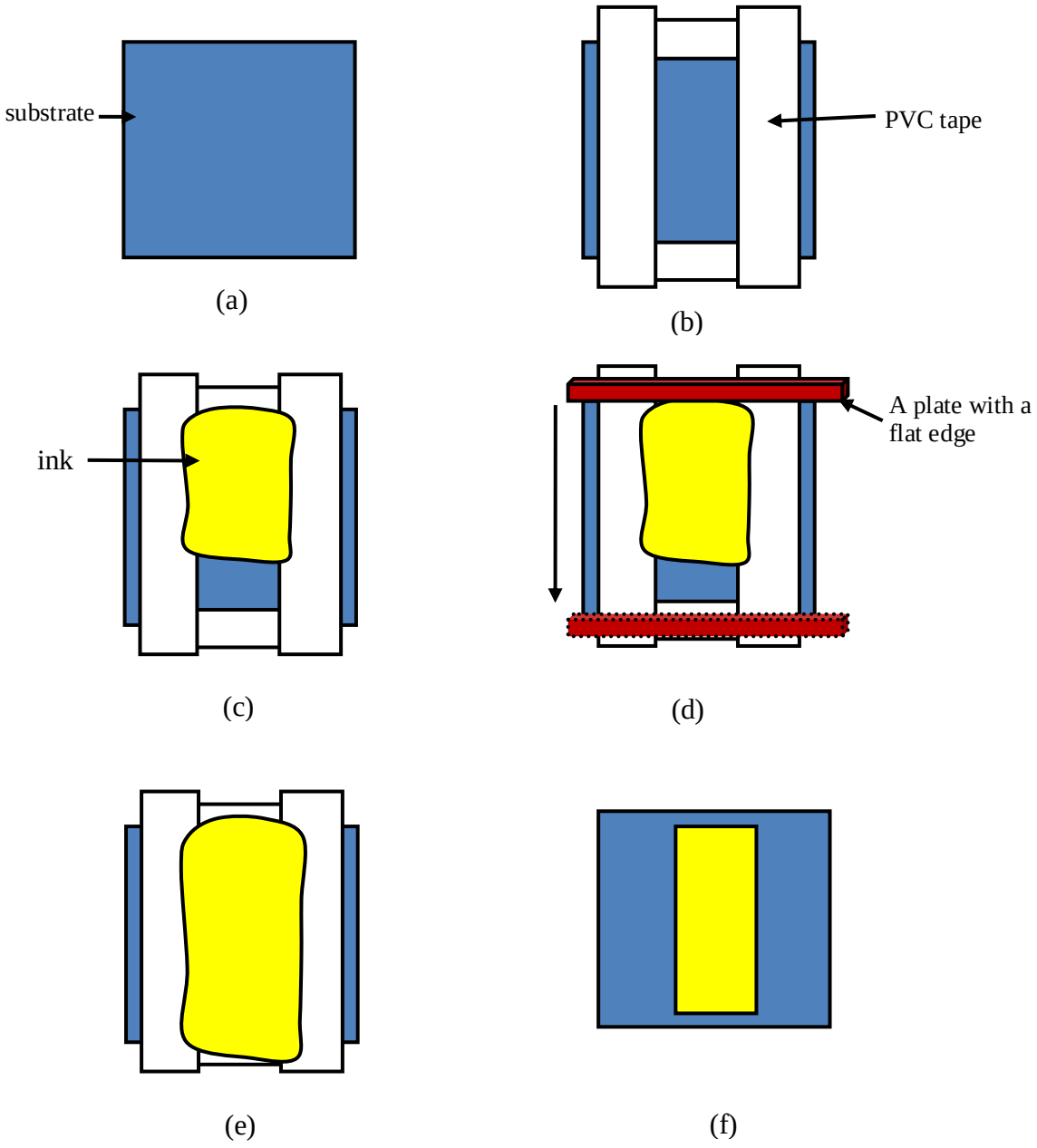

Figure 4.1: A schematic diagram of the doctor blading process. (a) A blank substrate. (b) Four strips of PVC tapes were applied onto the substrate to define a rectangular deposition area. (c) Some ink was placed in the deposition area. (d) A plate with a flat edge was used to scrape the ink into a flat surface and fill the whole deposition area with the ink as shown in (e). (f) The tapes were peeled off and a rectangular ink area remained on the substrate.

The manufacturing processes of a typical thick film sample on a silicon substrate were as follow. Firstly, silver ink was doctor bladed on the back side of a silicon substrate. A small amount of silver ink was brushed across the edge of the substrate so the back electrode could

be connected to the front bottom electrode. Then the sample was dried in an oven at 80 ℃ for 20 minutes. After drying, silver ink was doctor bladed on the front side of the silicon substrate as the bottom electrode which was connected to the back electrode through the silver brushed on the edge. Then the sample was dried at 80 ℃ for 20 minutes. Following that, PZT ink was doctor bladed on the bottom electrode on the front side and dried in the same condition as above. Finally, silver ink was doctor bladed on the PZT layer. Care must be taken to make sure it is insulated from the bottom electrode. In the doctor blading process of the three layers, PVC tapes were used to define the area and thickness of the layers. The sample was dried again and then ready for sintering. Schematic diagrams of the manufacturing process and the final structure are shown in Figure 4.2 and Figure 4.3 respectively.

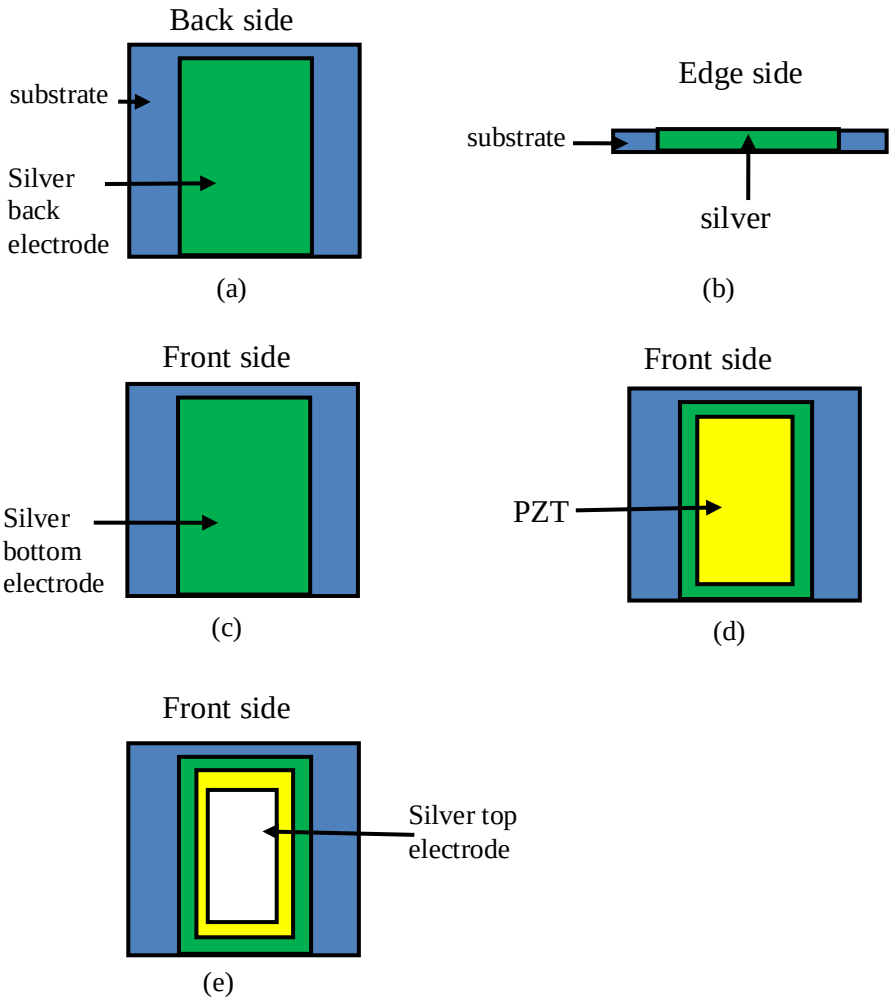

Figure 4.2: A schematic diagram of the manufacturing process of a thick film sample on a silicon substrate. (a) Silver ink was doctor bladed on the back side of a silicon substrate. (b) Silver ink was brushed across the edge of the substrate. (c) Silver ink was doctor bladed as a bottom electrode on the front side of the substrate. (d) PZT ink was doctor bladed on the bottom electrode. (e) Silver ink was doctor bladed as a top electrode on PZT.

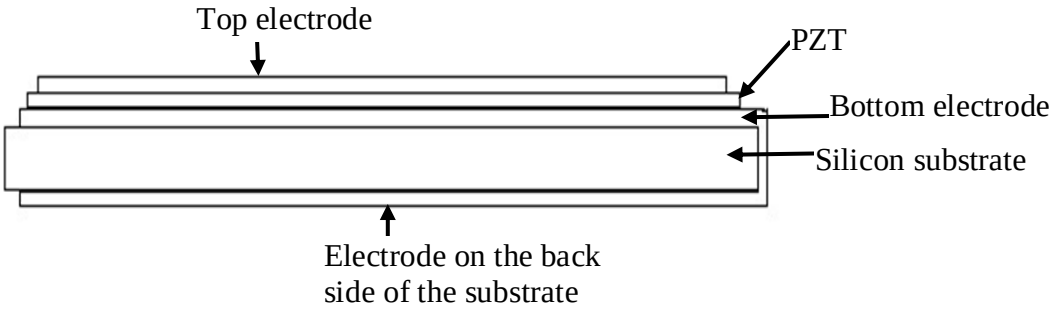

Figure 4.3: A schematic diagram of the final structure of a thick-film PZT sample on a silicon substrate.

4.2.3 Sintering

The next process was sintering. There were two kinds of sintering, co-sintering all three layers at one time and step-by-step sintering. For the sample described in Section 4.2.2 the co-sintering method was used. The furnace used was a 1600℃ muffle furnace (Serial No. 3967, Lenton). The sample was placed in an alumina crucible and covered by an alumina lid. The temperature rose from room temperature to 500 ℃ at a rate of 1 ℃/min, with 30 min dwells at 325℃ and 500℃ respectively, to burn out the organic vehicle in the silver and PZT inks. Then the temperature rose at a rate of 5 ℃/min to the peak temperature of 900 ℃, and dwelled for 60 min to sinter PZT into dense ceramic. Finally, it decreased at a rate of 5℃/min to room temperature.

4.2.4 Poling

Oil poling method was used to pole the thick-film samples. In oil a higher voltage can be applied than in air. In this study the active samples were all poled with a voltage of 1 kV (equivalent to a field strength of about 6.8 MV/m). The poling setup used is a home-made one. It consists of an oil container, a clamp, a high voltage supply (Model No. 3807, alpha Ⅲ brandenburg) connected to the clamp, a controllable heater and a temperature sensor. The samples were poled at 110 ℃ for 10 min.

4.2.5 Gold sputtering

For some samples, gold was sputtered onto sintered PZT to form the top electrode. Before gold sputtering, PVC tapes were applied to samples to shelter the areas which gold was not to be sputtered on and expose the areas which gold was to be sputtered on. After sputtering, tapes would be peeled off. This method was simpler and quicker than doctor blading a silver

film so it was used in some samples. The sputtering was performed with a peltier cooled sputter coater (Emitech K575 sputter coater, Emitech Ltd., Ashford, UK). Firstly, chromium was sputtered at a current of 100 mA for one cycle of 2 minutes. The sputtering speed of chromium was about 20 nm/min. Therefore, the thickness of the chromium layer was about 40 nm. Then gold was sputtered at a current of 80 mA for 2 cycles of 2 minutes. The sputtering speed of gold was about 50 nm/min. Thus, the thickness of the gold layer was about 200 nm.

4.3 Characterisation techniques for thick film PZT

4.3.1 Tape test of adhesion

For thick-film samples, the adhesion of the film material to the substrate is very important. The adhesion can be tested using a tape test in which a strip of PVC tape was applied on to a film on a substrate and then peeled off. The amount of material removed by the tape gives an indication of the adhesion of the material to the substrate. Tape tests have been used by other researchers to assess the adhesion of films to substrates [34]. Conventionally, if any of the film material is removed with the tape, it is considered to have failed the test.

4.3.2 Impedance Analysis

Impedance analysis was performed with an Agilent 4294A impedance analyser (Agilent Technologies UK ltd., Wokingham, UK). Impedance analysis can show the impedance-frequency spectrum of the measured sample. As resonance peaks and anti-resonance peaks in the impedance-frequency spectrum are typical characteristics of active piezoelectric material, the impedance analysis can be used to check if a sample has piezoelectric properties. Besides, the impedance analyser can measure some other parameters of materials, such as capacitance

and dissipation factor. Capacitance can be used to determine the dielectric constant ε_r of a material according to Equation (4.1), if the dimensions of the material are known.

$$\varepsilon_r = \frac{Cd}{S\varepsilon_0} \tag{4.1}$$

ε_r is the dielectric constant of the piezoelectric material, C is the capacitance of the thick film sample, d is the thickness of the PZT thick film, S is the surface area of the PZT thick film, and ε_0 is the permittivity of vacuum, $\varepsilon_0 = 8.854 \times 10^{-12}$ F/m.

The impedance analyser should be calibrated every time it is started or the range of measure frequency is changed. A holding jig is connected with the analyser for holding samples. One electrode of the jig is a metal platform on which the sample will be placed. The other electrode of the jig is a metal pin which can be moved up and down. The pin will be moved up to allow the sample to be placed on the platform and then move down into contact with the upper surface of the sample.

4.3.3 Measurement of Piezoelectric Coefficient d_{33}

The piezoelectric coefficient d_{33} is a characteristic parameter indicating the degree of activity of a piezoelectric material. In this project, d_{33} was measured with a d_{33} meter (YE 2730A, Sinocera). The principle of the d_{33} meter is that it applies a stress to the sample and measures the charges generated on the two sides of the sample then determine d_{33} using Equation (2.1). The d_{33} meter was calibrated using a standard sample with a known d_{33} value before it was used to measure experimental samples.

4.3.4 Scanning Electron Microscopy

Scanning Electron Microscopy (SEM) was used to observe and take pictures of the microstructure of materials such as PZT, silicon, silver, platinum and powders. The

microstructure of PZT explains why some PZT has higher piezoelectric performance than the others. Generally speaking, the denser the microstructure of PZT, the higher piezoelectric performance it has.

To make a sample suitable for SEM observation, it was glued onto a steel stub with a black round double-side pasty graphite tape. If the fracture of a sample was to be observed the sample needed to be placed vertically on the tape with the fracture facing upwards. One could use superglue to fix the sample on the tape. Then the sample and stub were placed in the sputter coater to deposit a thin layer of gold on them to make them electrical conductive.

In the present work, JEOL6060 and PHILIPSXL-30 were used to carry out SEM observations.

4.3.5 X-ray Diffraction (XRD)

X-ray Diffraction (XRD) is a non-destructive analytical technique which reveals information about the crystal structures of materials. When a beam of x-rays whose wavelengths are similar to the distance between crystal lattice planes strikes a crystalline solid, reinforced x-ray diffraction peaks of different intensities can be generated. The most commonly used x-ray diffraction method is the powder method because in a powder there is a random orientation of many particles to ensure that some of the particles are oriented in the x-ray beam to fulfill the diffraction conditions of Bragg's law.

In this project XRD was used to judge if any new phase or material emerge after sintering of PZT. In the XRD pattern of a sample consisting of a few layers of different materials, the whole pattern is the superimposition of patterns of different materials. The XRD machine used in this project was Equinox-3000, Inel. XRD analyses were performed with two thick film samples (Si/Ag/PZT/Au and Al_2O_3/silver/PZT/silver), the starting PZT powders (TRS

610C, batch 2002 and batch 2008 respectively), alumina substrates, powdered silicon substrates, and silver and gold electrodes.

Chapter 5 RESULTS AND DISCUSSION

In this chapter Section 5.1－5.3 are preliminary studies, including studies on the adhesion of electrode layers to substrates, PZT samples fabricated using dry ball-milled powders, and wet ball-milling of powders. Then Section 5.4－5.6 presents studies on thick-film PZT made using wet ball-milled powders.

5.1 Tape test of adhesion of electrode layers to substrates

It is a prerequisite for a thick-film device to be established that the electrode layers have good adhesion to the substrate. Therefore the adhesion of silver and platinum electrode materials to silicon and alumina substrates was tested using tape tests as described in Section 4.3.1. Platinum electrode was considered as one of potential electrodes because it has higher melting point (1773 ℃) than silver (962 ℃) and thus can withstand higher sintering temperature which may results in better sintering and piezoelectric properties of PZT. If any of the doctor bladed film material can be peeled off with adhesive tapes then it was considered to have failed the test. Otherwise it was considered to have passed the test. Sintered and green electrode materials on substrates were tested and the results are shown in Table 5.1 and Table 5.2 respectively. The electrodes were sintered at 900 ℃ for 10 minutes.

Table 5.1: Results of tape tests for adhesion of sintered electrodes to substrates. The electrodes were sintered at 900 ℃ for 10 minutes.

substrate / Electrode	Al_2O_3	Si
Ag	pass	pass
Pt	fail	pass

Table 5.2: Results of tape tests for adhesion of green electrodes to substrates

substrate / Electrode	Al_2O_3	Si
Ag	fail	pass
Pt	pass	fail

It is shown that sintered silver has good adhesion to both silicon and alumina substrates. In contrast, green silver has bad adhesion to alumina but still has good adhesion to silicon. Sintered platinum layers have good adhesion to silicon but bad adhesion to alumina. For green platinum layers the test results are opposite, bad adhesion to silicon and good adhesion to alumina. In practical experiments electrode layers will be sintered thus the results of sintered layers are more relevant.

5.2 Manufacturing and characterisation of thick-film samples made using dry ball-milled powders

5.2.1 Comparison of different sintering regimes of platinum electrode layers

Three different sintering regimes for platinum layers on silicon substrates were explored: (a) 900 ℃, 10 min. (b) 1000 ℃, 10 min. (c) 900 ℃, 20 min. As thick-film PZT was reported to be sintered around 900 ℃ in some literature [13], platinum electrodes for thick-film PZT in this study were firstly tried to sinter at 900 ℃ for 10 min (regime(a)). Then the sintering temperature and time were increased respectively to optimise the sintering regime (regime (b) and (c)). SEM pictures were taken to observe the microstructure of platinum to decide which regime is the optimum. Figure 5.1 shows the SEM pictures. Figure 5.1(a) shows both platinum and PZT layers which were step-by-step sintered. The upper half of Figure 5.1(a) is platinum and the lower half is PZT. The platinum sintered following regime (a) is very porous, and the porosity of platinum in the centre and that of platinum at the transition from platinum

to PZT are the same. Similarly, as can be seen in Figure 5.1(c), the microstructure of platinum sintered following regime (c) is porous as well. In contrast, platinum sintered using regime (b) is much denser. Therefore, it will probably have smaller electrical resistance and will more effectively prevent the lead in PZT layers from diffusing into silicon. Thus regime (b) was the optimum one for sintering platinum on silicon.

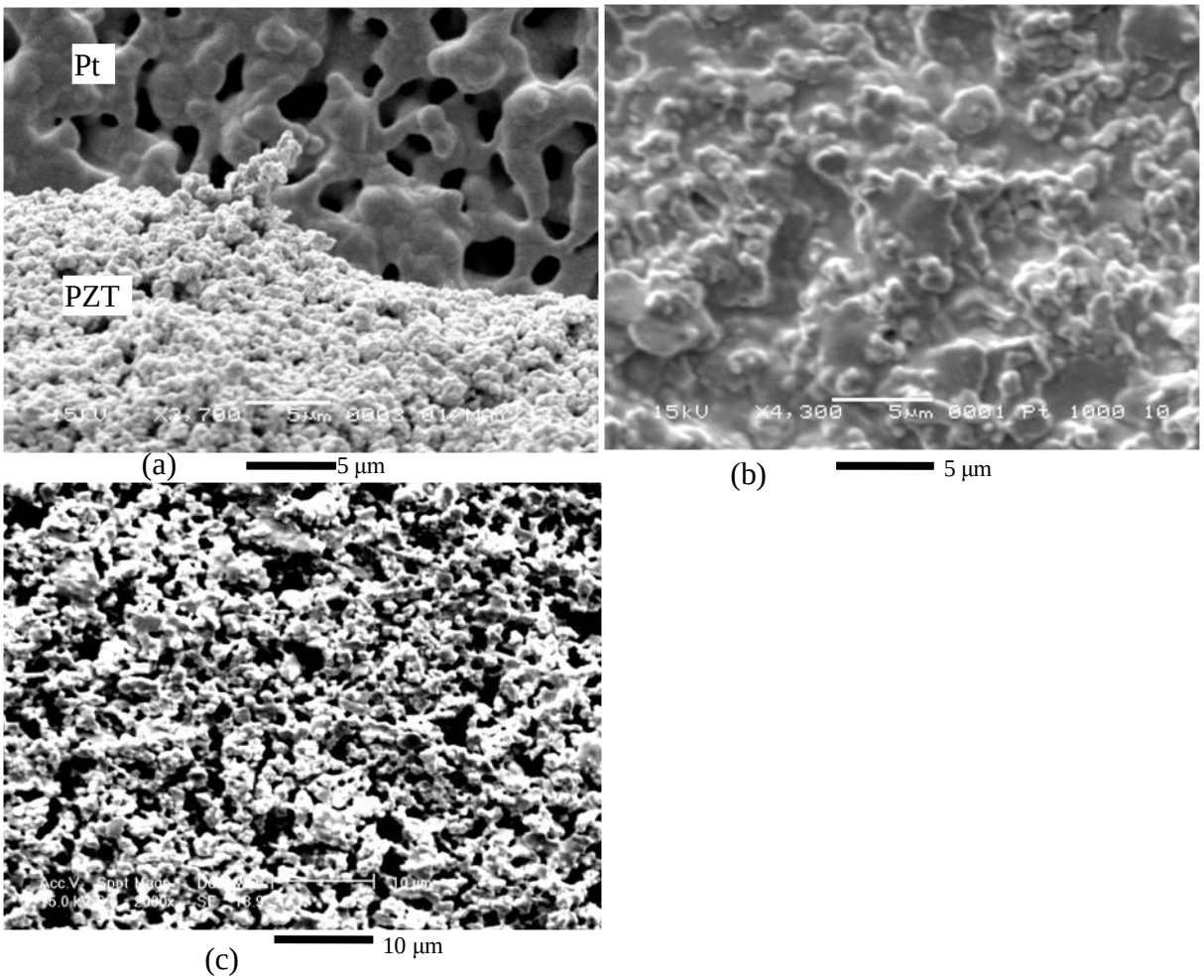

Figure 5.1: SEM pictures of platinum layers sintered on silicon substrates using three different sintering regimes. (a) 900 ℃, 10 min (the upper half is platinum, the lower half is PZT). (b) 1000 ℃, 10 min. (c) 900 ℃, 20 min.

5.2.2 Group 1 Samples

After testing of the electrodes as reported above, the first group of capacitor structure samples were made by a doctor blading method. The starting powders were 1 wt% borosilicate glass

and 99 wt% PZT powder (TRS 610C). The powders were only dry ball-milled without adding distilled water and zirconia milling media. After that, the powders were mixed with 20 wt% organic vehicle and processed using a three-roll mill as described in Section 4.2.1.

The main objective of the investigation was to fabricate PZT films on silicon substrates, but corresponding samples on alumina substrates were also made for comparison purposes. To investigate which sintering method was better, two sintering methods were explored: (1) sintering the bottom electrode layer first, and then depositing the PZT layer and sintering it (i.e. step-by-step sintering), and (2) co-sintering the two layers at one time. Samples sintered using each method were made. In addition, two possibilities of bottom electrodes (silver and platinum) were also explored to see which material was better to be the barrier layer preventing lead from diffusing into silicon. In summary, there were three variables and each variable had two possibilities. Thus eight samples were made in Group 1 and they are described in Table 5.3. All the PZT of the samples in Group 1 were sintered at 900 ℃ for 30 minutes. The top electrodes of them were sputtered gold. In this group the Pt electrode in the step-by-step sintering method was sintered at 900 ℃ for 10 min.

Table 5.3: Descriptions and d_{33} measurement results of samples in Group 1. All the samples were sintered at 900 ℃ for 30 minutes. The top electrodes were sputtered gold. The glass content in starting powders was 1 wt%. The powders were only dry ball-milled.

No. of sample	Bottom electrode	Sintering method	substrate	d_{33}/pCN^{-1}
1	Pt	Step by step	Silicon	Short circuited
2	Pt	Step by step	Alumina	Short circuited
3	Pt	Co-sinter	Silicon	14
4	Pt	Co-sinter	alumina	14
5	Ag	Step by step	Silicon	14
6	Ag	Step by step	Alumina	17
7	Ag	Co-sinter	Silicon	Short circuited
8	Ag	Co-sinter	alumina	Short circuited

After sintering, the samples were poled in an oil bath at 120 ℃ for 10 minutes. The electric field applied was 3 V/μm. As shown in Table 5.3, four samples were short circuited between top and bottom electrodes when being poled. This was indicated by the large current indicated on the voltage supply. Normally during the poling process the current reading should be nearly zero because piezoelectric materials are insulators. The other four samples which were successfully poled were used to do d_{33} measurement and impedance analysis. None of them showed resonance or anti-resonance peaks. Their d_{33} values were very small (14 or 17 pC/N).

This evidence demonstrated that the thick-film samples in Group 1 were not active. The reason might be the piezoelectric layer was too porous and there were some micro passages across the piezoelectric layer connecting the top and bottom electrodes. The porous microstructure of the piezoelectric layer is shown in an SEM picture in Figure 5.2. When a high voltage was applied between the top and bottom electrodes, the passage was electrically broken down and there was a big current through it. Besides, the short circuits could also be caused by sputtered gold going through porous PZT. The great porosity of the piezoelectric layers caused the bad piezoelectric property.

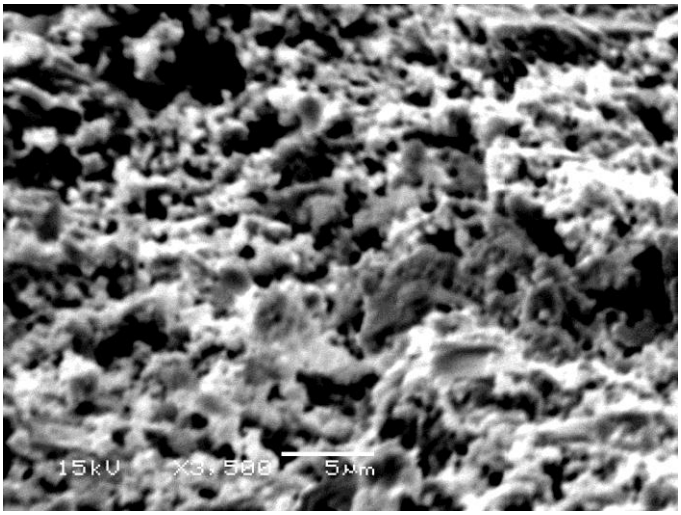

Figure 5.2: An SEM picture of a PZT thick-film layer of a typical sample in Group 1. It indicates that the microstructure of PZT was very porous and not well sintered.

5.2.3 Group 2 Samples

As the low yield of poling process and poor piezoelectric performance of the Group 1 samples were due to porous microstructure, methods needed to be proposed to improve the density of the thick-film PZT. There are three potential methods to improve the density of the sintered PZT layers. The first one is to increase the sintering temperature. Normally bulk PZT is sintered at 1200 ℃ to obtain dense material. However, at such high temperature, lead in PZT will diffuse into silicon, react with silicon and produce a lead silicate which will inhibit subsequent etching process. Besides, diffusion of lead reduces the lead content in PZT and therefore reduces the piezoelectric activity of PZT. Thus the sintering temperature for thick-film PZT on silicon substrates should be limited around 900 ℃. Increasing temperature is not a good method.

The second method is to increase the glass content in the starting powders. The glass acts as a binder and forms a bonding matrix during the sintering process. Therefore more glass could improve sintering and densification. The third method is to increase the sintering time.

In addition, there is another method to improve the performance of the PZT films. It is to put the samples on a layer of lead oxide sand in a covered crucible during the sintering process. Lead oxide is volatile at high temperatures so there will be some loss of lead oxide in sintering process. The lead oxide sand helps to maintain the lead stoichiometry in PZT and therefore helps retain its piezoelectric properties.

Following the discussion above, a second group of samples were made. The samples in Group 2 are described in Table 5.4. The glass content in the starting powders was increased to 3 wt%. The powders were still dry ball-milled as the same with Group 1. Group 2 focused on platinum bottom electrode and silicon substrate. The sintering temperature used was still 900 ℃, the same as that used in Group 1. The step-by-step sintering method was employed in Group 2. It is worth mentioning that the sintering temperature for platinum layers was 1000 ℃ because platinum sintered at 1000 ℃ is denser than that sintered at 900 ℃ (as described in Section 5.2.1). The top electrodes were still sputtered gold.

No. 1 sample was sintered in lead oxide sand (meanwhile keeping the other conditions the same with No. 3 and No.4 samples) to investigate the effect of sintering with lead oxide sand. No. 2 sample was sintered for 60 minutes (meanwhile keeping the other conditions the same with No. 3 and No. 4 samples) to study if longer sintering time can improve the performance of the piezoelectric thick film.

After sintering the samples were poled in the same condition as Group 1. This time they were all successfully poled. Then impedance analysis and d_{33} measurement were done with them. None of them showed resonance peaks but they had bigger values of d_{33} than those of group 1 (see Table 5.4). Sintering with lead oxide sand improves the d_{33} slightly (as seen with No. 1

sample), and increasing sintering time even reduces d_{33} (as seen with No. 2 sample). However, there is still some disparity between the d_{33} of samples in Group 2 and the d_{33} reported in literature [10] (50 pC/N). In literature [10] the sample was made from 96 wt% PZT 501A powder and 4 wt% Li_2CO_3 and Bi_2O_3 glass powder. It was fired at 850℃ for 15min.

Table 5.4: Descriptions and d_{33} measurement results of samples in Group 2. The Pt bottom electrodes were sintered at 1000 ℃ for 10 min. The top electrodes were sputtered gold.

No.	Bottom electrode	Sintering method	substrate	sintering temperature of PZT / ℃	Sintering time of PZT	If sintered in lead oxide sand	Average d_{33}/ pCN^{-1}
1	Pt	Step by step	silicon	900	30 min	Yes	32±1.6
2					60 min	No	20±1.2
3					30 min	No	29±1.4
4					30 min	No	26±1.3

SEM pictures were taken to observe the microstructure of PZT of these samples. The picture of No. 3 sample in Table 5.4 is shown in Figure 5.3. As can be seen in the figure, the microstructure of PZT is denser than that of samples in Group 1 (see Figure 5.2). This is why all the samples were successfully poled and showed higher d_{33} than samples in Group 1. But the microstructure of samples in Group 2 is still rather porous, and the absence of any measurable resonance peaks in the impedance plots was still a concern.

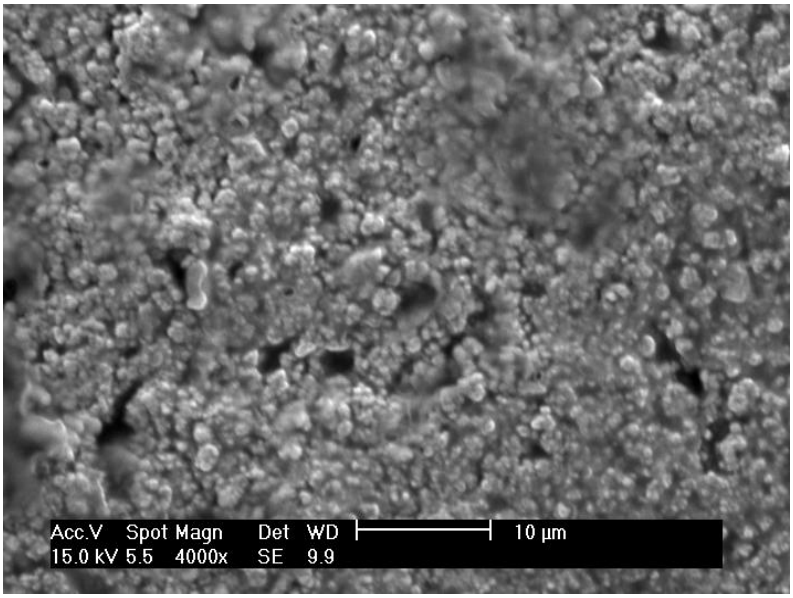

Figure 5.3: SEM picture of PZT of No. 3 sample in Group 2 made using dry ball-milled powders. The sample was sintered at 900 ℃ for 30 min. The microstructure shown is still very porous. But it is denser than samples in Group 1 as shown in Figure 5.2.

5.2.4 Group 3 Samples and Summary of Group 1-3

As the samples in Group 2 still had poor d_{33} values, a third group of samples was made using a higher sintering temperature (1000 ℃). The PZT ink, substrate, top and bottom electrodes and sintering method used for samples in Group 3 were the same as those used for samples in Group 2. But again, these samples did not show resonance peaks in the impedance plots. They showed very low d_{33} values, with an average value of 30 ±1.5 pC/N. All the first three groups of samples are summarized in Table 5.5.

Table 5.5: Summary descriptions of the three groups of initial test samples.

Group	1	2	3
Glass content in starting powders	1 %	3 %	3 %
Top electrode	Sputtered gold		
Bottom electrode	Pt or Ag	Pt	Pt
Peak sintering temperature of PZT	900 ℃	900 ℃	1000 ℃
Duration at peak temperature	30 min	30 min or 60 min	30 min or 60 min
Sintering method	Step-by-step sintering or co-sintering	Step-by-step sintering	Step-by-step sintering
substrate	Al_2O_3 or silicon	silicon	silicon

5.3 Wet ball-milling of starting powders

The three groups of samples in the initial series were made using dry ball-milled powder and did not have adequate piezoelectric performance. This may be because the dry ball-milled powder has too big particle sizes and large particles are difficult to be sintered. Wet ball-milling can reduce particle size because added distilled water increases the fluidity of the milled mixture and zirconia milling media cascade in the bottle breaking down agglomerates.

5.3.1 Particle Size and Surface Area Measurement

To demonstrate the effect of wet ball-milling, particle sizes were measured for the following four powder samples:

(1) as-supplied PZT powder (batch 2002)

(2) as-supplied PZT powder (batch 2008)

(3) dry ball-milled PZT powder (batch 2002)

(4) dry ball-milled PZT powder (batch 2008)

(5) wet ball-milled PZT powder (batch 2002)

(6) wet ball-milled PZT powder (batch 2008)

Surface areas were measured for the following three powder samples:

(1) as-supplied PZT powder (batch 2002)

(2) as-supplied PZT powder (batch 2008)

(3) borosilicate glass

The results are shown in Table 5.6. The powders are much agglomerated, so the measured particle sizes are actually agglomerate sizes. The measured particle sizes of the dry ball-milled PZT powders are almost the same as those of the corresponding as-supplied powders so they were not recorded. In the dry ball milling process, no solvent or milling media were used and the ball mill rotated slowly so it did not reduce the particle sizes.

d_{50} is the median of particle sizes. Conventionally it is used as the measured particle size. For the as-supplied powders, batch 2002 has smaller agglomerate size than batch 2008. Wet-ball milled powders have much smaller agglomerate sizes than the corresponding as-supplied powders. For batch 2002, it is reduced from 22.97 μm to 1.45 μm. For batch 2008, it is reduced from 30.62 μm to 1.67 μm. Wet ball-milled batch 2002 powder has smaller agglomerate size than wet ball-milled batch 2008 powder.

The BET surface area results do not contradict the agglomerate size results because the former refer to the surface area of the primary particles and the latter refer to the size of agglomerates each of which consists of many primary particles. The data mean that the as-supplied batch 2002 powder has smaller agglomerates, but bigger primary particles than its 2008 counterpart.

In addition, wet ball-milling also made the distribution of particle size narrower. As shown by Figure 5.4, wet ball-milled powder has narrower distribution of particle size than as-supplied powder. The as-supplied powder has a bi-modal distribution.

Table 5.6: Measured particle sizes and surface areas of powders

Powder sample	d_{50} / µm	BET surface area / m^2g^{-1}
As-supplied batch 2002	22.97	0.5903
As-supplied batch 2008	30.62	1.6225
Batch 2002 wet ball-milled	1.45	
Batch 2008 wet ball-milled	1.67	
Borosilicate glass		1.2119

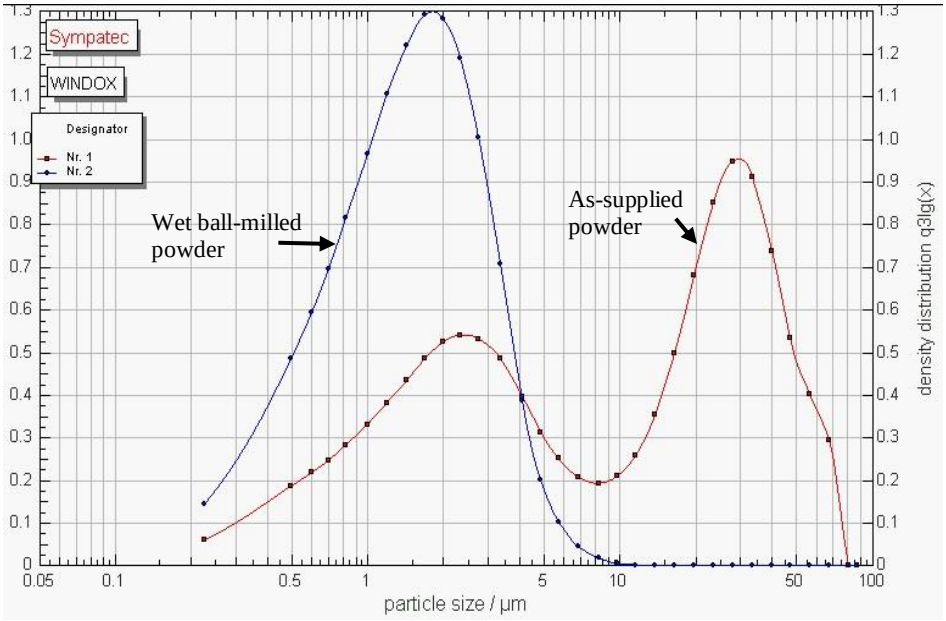

Figure 5.4: particle size distribution curves of as-supplied PZT batch 2002 powder and wet ball-milled PZT batch 2002 powder. The wet ball-milled powder has narrower distribution and more uniform particle size than the as-supplied powder.

5.3.2 SEM Pictures of Powders

SEM pictures were taken to observe the sizes and shapes of the powder particles including:

(a) as-supplied borosilicate glass powder

(b) as-supplied PZT powder (TRS 610C batch 2002)

(c) as-supplied PZT powder (TRS 610C batch 2008)

The pictures are shown in Figure 5.5. The glass powder particles have irregular shapes with sharp angles (see Figure 5.5(a)). There are agglomerates in the as-supplied PZT powder batch 2002 and batch 2008 (see Figure 5.5(b) and (c)). The batch 2008 powder is more agglomerated than batch 2002 powder. The size of agglomerates in batch 2008 powder is much bigger than that of agglomerates in batch 2002 powder. This is consistent with the results of measured particle sizes (actually agglomerate sizes) shown in Table 5.6.

(a)

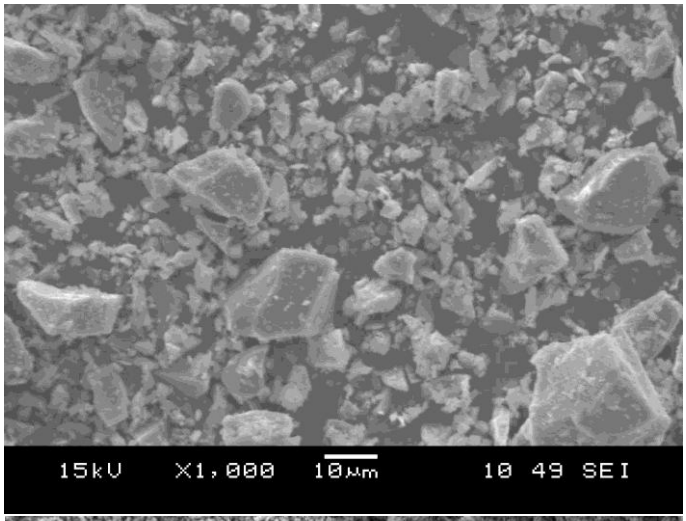

(b)

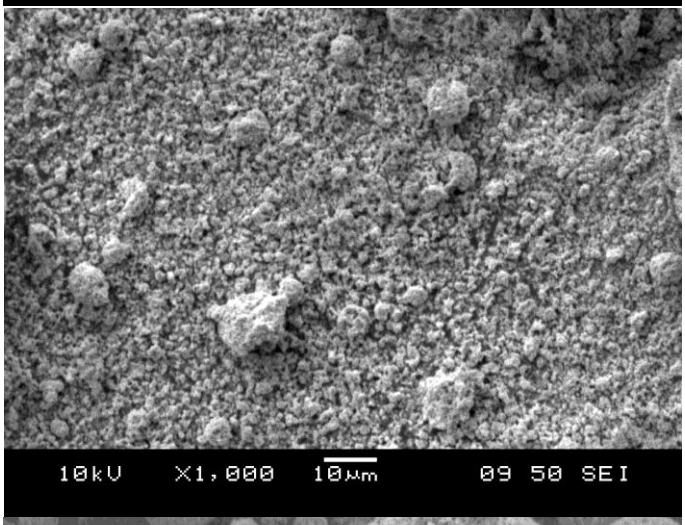

(c)

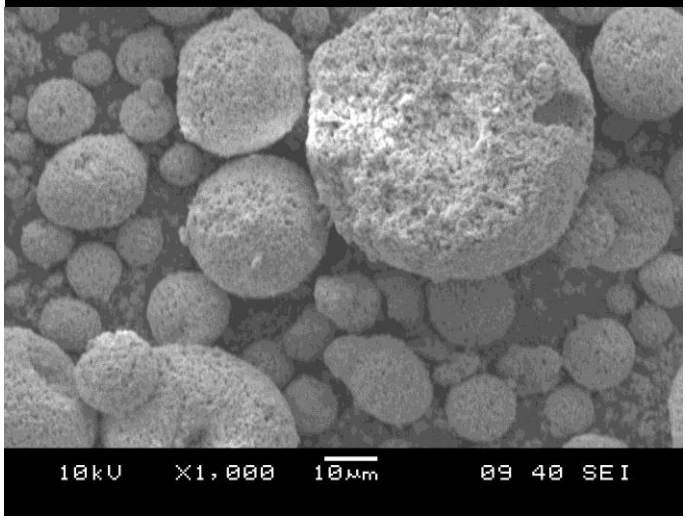

Figure 5.5: SEM pictures of (a) as-supplied borosilicate glass powder, (b) as-supplied PZT powder (TRS 610C batch 2002), and (c) as-supplied PZT powder (TRS 610C batch 2008).

In conclusion, wet ball-milling can break agglomerates in the powder and make the particle size distribution narrower. These advantages may lead to better thick-film PZT. Therefore, another batch of ink was made using wet ball-milled powder. The starting powders were 1 wt% borosilicate glass and 99 wt% TRS 610C powder (batch 2002). The manufacturing process is as described in Section 4.2.1.

5.4 Thick-film samples made using wet ball-milled powders

5.4.1 Thick-film samples on alumina substrates

Some thick-film samples were fabricated with the ink made using wet ball-milled powders. As thick-film PZT on alumina substrates had been investigated by several researchers and has been demonstrated to be mature and successful, some samples on alumina substrates were fabricated initially. The bottom and top electrodes were silver films. The sintering method employed was co-sintering the three layers at one time because in the step-by-step sintering process the PZT would be sintered twice and thus there would be more loss of lead at high temperature which would result in lower piezoelectric properties of the PZT. Lead oxide is volatile at high temperature. The sintering regime employed is described in Section 4.2.3. The temperature rose from room temperature to 500 ℃ at a rate of 1 ℃/min, with 30 min dwells at 325℃ and 500℃ respectively, to burn out the organic vehicle in the silver and PZT inks. Then the temperature rose at a rate of 5 ℃/min to the peak temperature of 900 ℃, and dwelled for 60 min to sinter PZT into dense ceramic. Finally, it decreased at a rate of 5 ℃ /min to room temperature.

After sintering, the samples were poled in an oil bath at 110 ℃ under a voltage of 1 kV for 10 min. This voltage was equivalent to an electric field of 6.8 MV/m because the thickness of the

PZT layer was measured as 146 μm (as will be described later in this section). All the samples were successfully poled. Then d_{33} was measured for the samples and the results are shown in Table 5.7. For each sample, d_{33} was measured at five different locations of the sample and then the average value and standard deviation were calculated. The average value of d_{33} for the three samples is 120±4.7 pC/N, which is higher than the d_{33} value reported in literature [8] (52 pC/N). In literature [8] the thick-film sample was made from a similar material PZT 5H and 10 wt% lead borosilicate glass. The powder was also ball milled and the paste was mixed using a three roll mill. The sample was fired at 890℃ for 34 min. More details are provided in Table 2.1. The lower literature value may be due to the higher glass content and the shorter firing time.

Table 5.7: d_{33} measurement results of thick-film samples on alumina substrates made using wet ball-milled powders. Each sample was measured five times at different locations of the sample. Average d_{33} and standard deviation were calculated for each sample and all the samples together.

No. of sample	Average d_{33} and standard deviation of each sample / pCN^{-1}	Average d_{33} and standard deviation of all samples / pCN^{-1}
1	118±15.5	120±4.7
2	116±8.2	
3	125±16.8	

The samples were also characterised by impedance analysis. They all showed clear resonance and anti-resonance peaks in their impedance-frequency plots. A typical impedance-frequency plot and a typical phase-frequency plot are shown in Figure 5.6. There are three pairs of resonance and anti-resonance peaks in the impedance curve. A resonance peak is where the impedance reaches a local minimum value. An anti-resonance peak is where the impedance reaches a local maximum value closely after a resonance peak. At a frequency where a pair of resonance and anti-resonance peaks occurs, a corresponding peak also occurs in the phase

curve. The first three pairs of peaks from left to right correspond to the length, width and thickness of the PZT layer respectively. The resonance frequencies are 3.057, 4.619, and 8.446 MHz respectively. The second peak is split into two peaks probably because the edge of the layer is not flat or the width of the layer is not uniform.

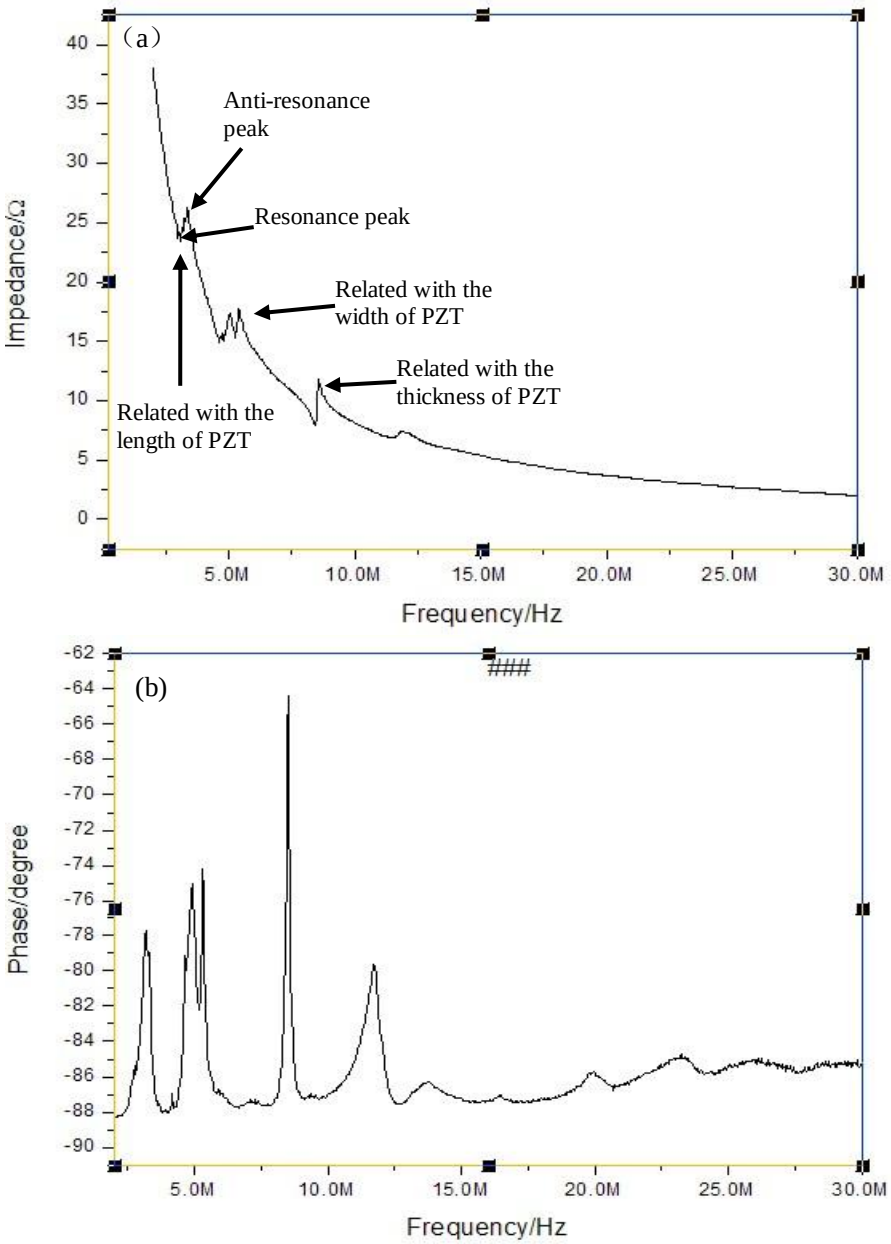

Figure 5.6: A typical impedance-frequency plot (a) and a typical phase-frequency plot (b) of a thick-film sample on an alumina substrate. There are three pairs of resonance and anti-resonance peaks from left to right in the impedance curve, corresponding to the length, the width, and the thickness of the PZT layer respectively.

The resonance and anti-resonance frequencies in Figure 5.6 were recorded and the effective electromechanical coupling coefficient k_{eff} was calculated using the equation:

$$k_{eff} = \frac{\sqrt{f_a^{\,2} - f_r^{\,2}}}{f_a} \qquad (5.1).$$

f_a is the anti-resonance frequency and f_r is the resonance frequency. The coefficient k_{eff} is defined as follows:

$$k_{eff}^2 = \frac{\text{electrical energy converted to mechanical energy}}{\text{input electrical energy}} \quad (5.2)$$

As can be seen in Table 5.8, k_{eff} related with the length and the width of the sample are similar, possibly because they are both perpendicular to the poling direction. These two values are much greater than the k_{eff} related with the thickness of the sample, which is along the poling direction.

Table 5.8: Three pairs of resonance and anti-resonance frequencies in Figure 5.6 and corresponding k_{eff}.

No. of frequency	Resonance frequency / MHz	Anti-resonance frequency / MHz	k_{eff}
1	3.057	3.344	0.41
2	4.619	5.010	0.39
3	8.446	8.576	0.17

Some other parameters of the samples were also measured using the impedance analyser, including capacitance at 1 kHz and dissipation factor at 1 kHz (see Table 5.9). The length and width of the PZT layers were measured with a micrometer. The thickness of the PZT layer was measured as 146 μm from the SEM micrograph (see Figure 5.7). In this picture, the gold top electrode is very thin (approximately 240 nm) so its thickness can be estimated. Then the relative permittivity of the samples were calculated using equation (4.1) and shown in Table 5.9. The average relative permittivity is 657 ±16.8. Then dielectric Q factor is calculated as the reciprocal of dissipation factor. The results are shown in Table 5.9.

Table 5.9: Capacitance, length, width, relative permittivity, dissipation factor and dielectric Q factor at 1 kHz of three samples.

No. of sample	Cs at 1 kHz / pF	Length/ mm	Width/mm	Relative permittivity	Dissipation factor at 1 kHz/ 10^{-3}	Dielectric Q factor
1	1207	11.67	2.57	664	21.9	45.7
2	1390	12.10	2.97	638	23.9	41.8
3	1378	11.87	2.86	669	26.0	38.5

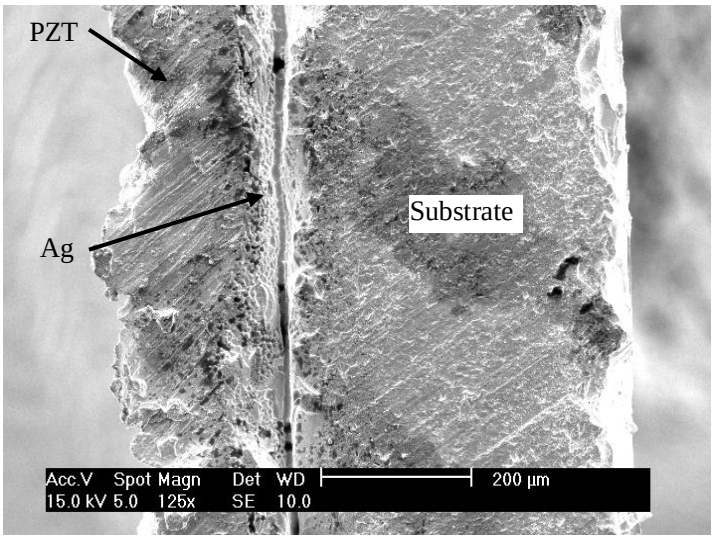

Figure 5.7: an SEM picture used for measuring the thickness of the PZT layer. The gold top electrode is very thin (approximately 240 nm) so its thickness can be estimated in this picture.

The increased measured d_{33} value and the resonance peaks in the impedance-frequency plot demonstrate that these samples are piezoelectric. Thus wet ball-milling is demonstrated to improve the performance of the samples greatly. The whole manufacturing process of the thick-film samples is proven to be successful.

5.4.2 Thick-film samples on silicon substrates

As the manufacturing process of thick-film samples had been proven to be successful on alumina substrates, the focus of study was returned to thick films on silicon substrates because the final application would be on silicon substrates. Three thick-film samples on silicon substrates were made by doctor blading method. The PZT ink used was made from wet ball-milled powders consisting of 1 wt% borosilicate glass and 99 wt% PZT powder. The

top electrodes were sputtered gold instead of sintered silver films. The samples were sintered at 900 ℃ for 1h using the same regime as described in Section 5.4.1. After that they were poled in an oil bath at 110 ℃ under a voltage of 1 kV for 10 min.

The piezoelectric coefficient d_{33} of the samples were measured and the results are shown in Table 5.10. Each sample was measured five times at a different location of the sample each time. The average value of d_{33} for three samples was 74±6.7 pC/N. It is higher than the value reported by literature [10] (50 pC/N, see Table 2.1 for details), in which the sample was made from 96 wt% PZT 501A powder and 4 wt% Li_2CO_3 and Bi_2O_3 powder. The sample was fired at 850℃ for 15min. The lower firing temperature and the shorter firing time may result in the lower d_{33}.

Meanwhile the average d_{33} of 74 pC/N is lower than the value reported in literature [9] (102 pC/N, see Table 2.1 for details), in which the sample was made from 95 wt% PZT 5H powder and 5 wt% lead borosilicate powder. The sample was fired at 800℃ for 8h. Although the firing temperature is lower than that used in this work, its firing time is much longer than that used in this work, which may result in the higher d_{33}.

In addition, the d_{33} 74 pC/N is much lower than the d_{33} 120 pC/N of thick-film samples on alumina substrates described in Section 5.4.1. This may be due to the reaction between silicon and the lead in PZT, which is also reported in literature [13].

Table 5.10: d_{33} measurement results of thick-film samples on silicon substrates. They were made using wet ball-milled starting powders and sintered at 900 ℃.

No. of sample	Average d_{33} and standard deviation for each sample / pCN^{-1}	Average d_{33} and standard deviation for all the samples / pCN^{-1}
1	78±6.3	74±6.7
2	77±2.5	
3	66±8.3	

Impedance analysis was carried out on the samples. All the three samples showed resonance peaks in their impedance-frequency plots. The impedance-frequency plot of No. 2 sample is shown in Figure 5.8. The resonance frequencies, anti-resonance frequencies and the effective electromechanical coupling coefficient k_{eff} of No. 2 sample are shown in Table 5.11. Capacitances, dissipation factors, and dielectric Q factors of the three samples are shown in Table 5.12.

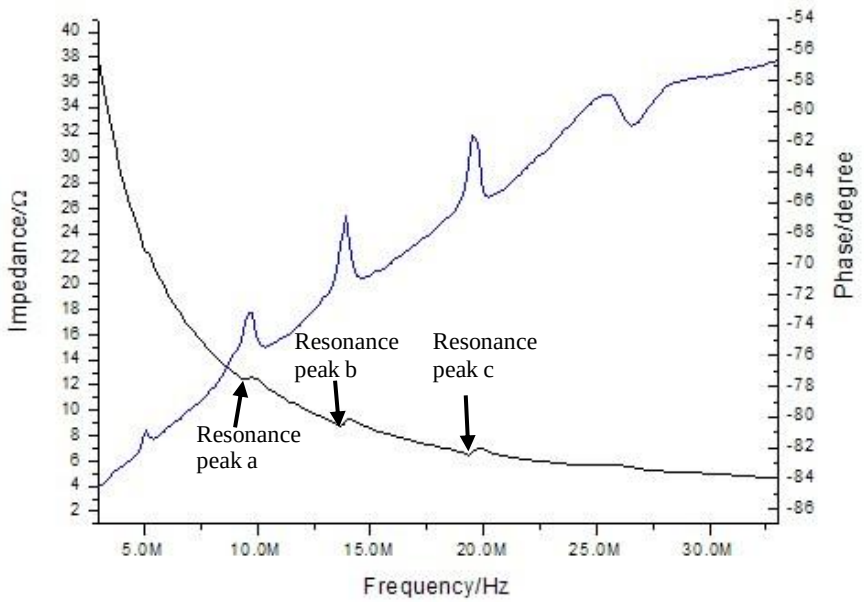

Figure 5.8: The impedance-frequency plot and phase-frequency plot of No. 2 sample in Table 5.10. The three pairs of resonance and anti-resonance peaks in the impedance curve (black curve) from left to right correspond to the length, width and thickness of the PZT layer respectively. The blue curve is the phase curve.

Table 5.11: Resonance frequencies, anti-resonance frequencies and k_{eff} of No. 2 sample in Table 5.10.

No.	Resonance frequency / MHz	Anti-resonance frequency / MHz	k_{eff}
a	9.392	9.754	0.27
b	13.613	14.095	0.26
c	19.341	19.884	0.23

Table 5.12: Capacitance at 1 kHz, dissipation factor at 1 kHz, dielectric Q factor, length, width and relative permittivity of the three thick-film samples on silicon substrates made using wet ball-milled powders.

No.	C_s at 1 kHz / pF	Length/mm	Width/mm	Relative permittivity	Dissipation factor at 1 kHz / 10^{-3}	Dielectric Q factor
1	1378	9.78	3.67	633	23.6	42.4
2	1603	10.03	4.12	640	23.2	43.2
3	979.5	7.37	3.59	610	24.5	40.8

The length and width of the PZT layer were measured using a micrometer. The thickness of the PZT layer was considered to be the same as that of the PZT layer on alumina substrate (146 μm) because the manufacturing processes are the same. Then the relative permittivity of the three samples were calculated using Equation (4.1). The results are shown in Table 5.12. The average relative permittivity of the three samples is 628 ±15.3.

An SEM picture of the fracture of PZT on silicon substrate made using wet ball-milled powders is shown in Figure 5.9. The microstructure of this PZT is much denser than that of PZT made using dry ball-milled powders shown in Figure 5.2 and Figure 5.3. This is due to the finer particles that wet ball-milling produces. Finer particles promote the sintering effect. From the perspective of energy, the drive for sintering is the reduction of surface energy of the particles. Finer particles have higher surface area and thus higher surface energy. Therefore, finer particles are easier to be sintered than large particles. In the sintering process, the matter of neighbouring particles must diffuse into each other and the time taken to finish this process is proportional to the square of the particle size [2]. The process will be

significantly slower if the particles comprise aggregates of crystals rather than individual crystals. Aggregates usually densify more quickly internally than with neighbouring aggregates, resulting in residue of pores in the spaces originally between the aggregates. This explains why PZT made using wet ball-milled powders has much better piezoelectric performance than that made using dry ball-milled powders.

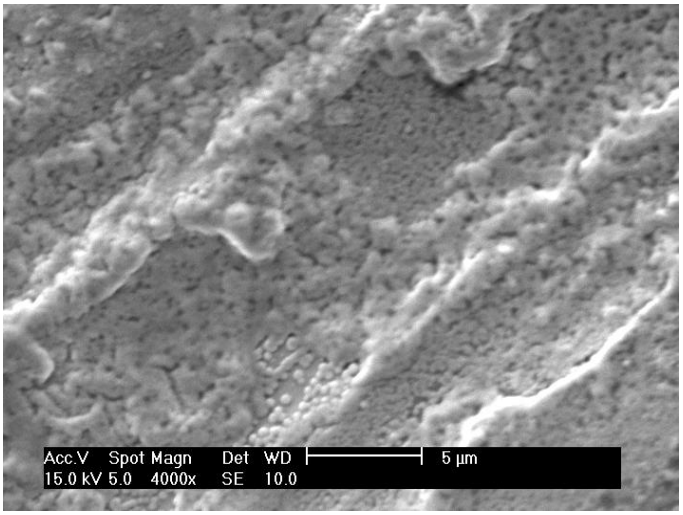

Figure 5.9: An SEM picture of the fracture of PZT on silicon substrate made using wet ball-milled powders. This sample was sintered at 900 ℃ for 1h and poled at 110 ℃ under 1 kV for 10 min. The microstructure of this sample is much denser than that of samples made using dry ball-milled powders shown in Figure 5.2 and Figure 5.3.

5.4.3 A study on different sintering temperatures for thick-film PZT on silicon substrates

The results of d_{33} measurement and impedance analysis of thick-film PZT on silicon substrates sintered at 900 ℃ demonstrate that the samples are piezoelectric. In order to investigate the effect of different sintering temperatures, two samples were sintered at 850 ℃ for 1h and another two samples were sintered at 950 ℃ for 1h. After the sintering at 950 ℃, one of the two samples stuck to the alumina plates under it in the crucible, probably because the silver on the back side of the silicon substrate melted at the peak temperature and stuck the silicon to the alumina plate (The melting point of silver is 961.8 ℃). The sample stuck to the

alumina plate could not be taken off and thus could not be poled and characterised. But the other sample was not stuck to the alumina plate and was taken off easily. This indicates that the temperature distribution in the furnace is not homogeneous.

d_{33} measurement results of the three samples are shown in Table 5.13. An average d_{33} value of 76 pC/N was obtained with the two samples sintered at 850 ℃. An average d_{33} value of 79 pC/N was obtained with the sample sintered at 950 ℃. Both of the values are close to that of the samples sintered at 900 ℃ (74 pC/N). All the three samples show resonance and anti-resonance peaks in their impedance-frequency plots (see Figure 5.10). This means sintering temperature does not have significant influence on the piezoelectric properties in the range from 850 to 950 ℃. However, lower sintering temperature is quicker to reach and quicker to cool down as well. It also saves energy. Therefore, from the perspective of time and energy-saving, a lower sintering temperature of 850 ℃ is recommended.

Table 5.13: Results of d_{33} measurement for two samples sintered at 850 ℃ and one sample sintered at 950 ℃. Their bottom electrodes were silver and their top electrodes were sputtered gold.

No.	Sintering temperature / ℃	Average d_{33} of each sample / pCN^{-1}	Average d_{33} of samples / pCN^{-1}
1	850	79±4.7	76±4.9
2	850	72±11.0	
3	950	79±8.9	79±8.9

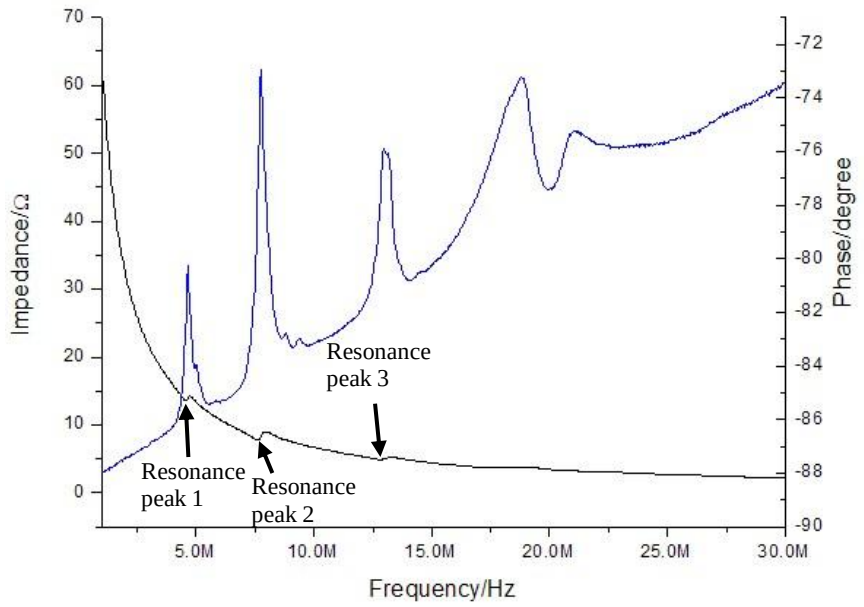

Figure 5.10: Impedance-frequency plot of No.2 thick-film sample on silicon substrate sintered at 850 ℃. The black curve is the impedance curve and the blue curve is the phase curve.

Then several samples with platinum bottom electrodes were made to see if they have better performance than those with silver bottom electrodes. Two samples were sintered at 900 ℃ for 1h. However, after sintering, PZT thick films upwraped off from platinum electrodes and were easily broken in subsequent processes. This indicates that platinum is not suitable for being bottom electrode for thick-film PZT on silicon substrates.

5.5 X-ray Diffraction (XRD)

To study if new material or phase was produced in the sintering process, XRD analyses were done with the following samples:

(1) an active thick film PZT sample on a silicon substrate (Si/Ag/PZT/Au) sintered at 900 ℃ for 1h.

(2) an active thick film PZT sample on an alumina substrate (Al_2O_3/Ag/PZT/Ag) sintered at 900 ℃ for 1h.

(3) ground silicon powder obtained from a silicon substrate

(4) an alumina substrate

(5) a layer of silver film on a silicon substrate

(6) a layer of sputtered gold film on a silicon substrate

(7) as-supplied PZT powders (TRS 610C batch 2002 and batch 2008)

(8) borosilicate glass powder.

Initially XRD analysis was also done for a silicon substrate which was a single crystal, but the patterns obtained were completely noises. It was because the single crystal was difficult to be oriented in the x-ray beam to satisfy the diffraction conditions of Bragg's law. Then the silicon substrate was ground into powder and then analysed with XRD. This time a good XRD pattern with clear peaks was obtained because in the powder there was a random orientation of many particles to ensure that some of the particles were oriented in the x-ray beam to satisfy the diffraction conditions.

The XRD patterns were read using the software Match!. XRD patterns of PZT powder, thick-film samples on silicon and alumina substrates are shown in Figure 5.11. In the pattern of PZT powder, the peaks are labelled with the corresponding Miller indices of crystallographic planes of a perovskite structure. This was done according to XRD patterns of PZT from literature [35] and [36]. The patterns of thick-film samples were compared with those of its starting components (i.e. top and bottom electrode layers, PZT layer, and substrates). Every peak of the starting components was matched one-by-one manually to the corresponding peak of the thick-film samples. Each peak of the film samples is labelled with its source material(s). Please note that the silicon substrate in the film sample is single crystal so it generates noises rather than peaks in the XRD pattern Figure 5.11(b). Therefore in Figure 5.11(b), there is no peak belonging to silicon.

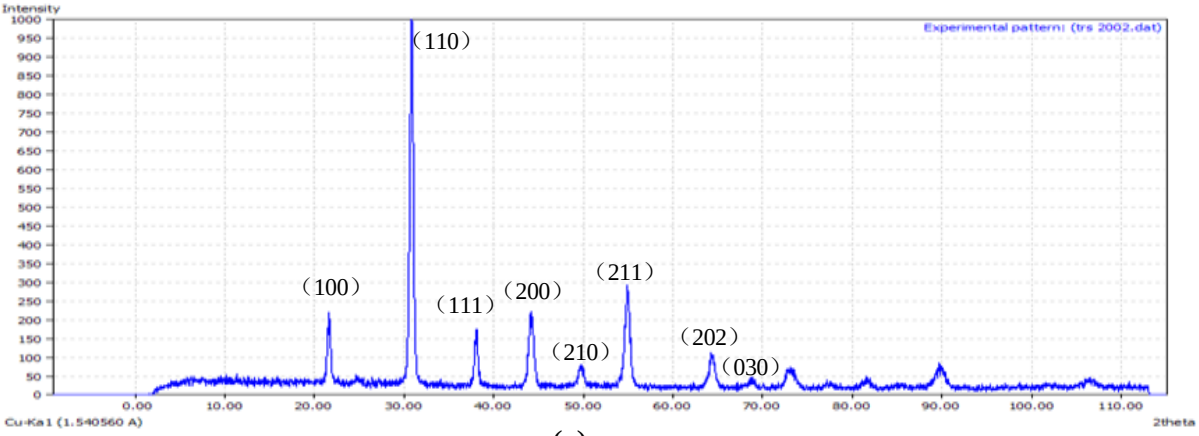

(a)

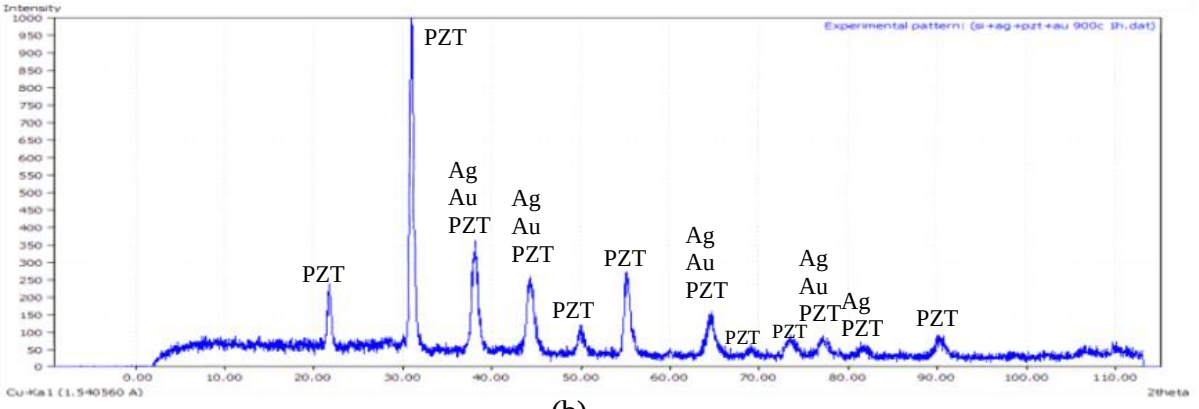

(b)

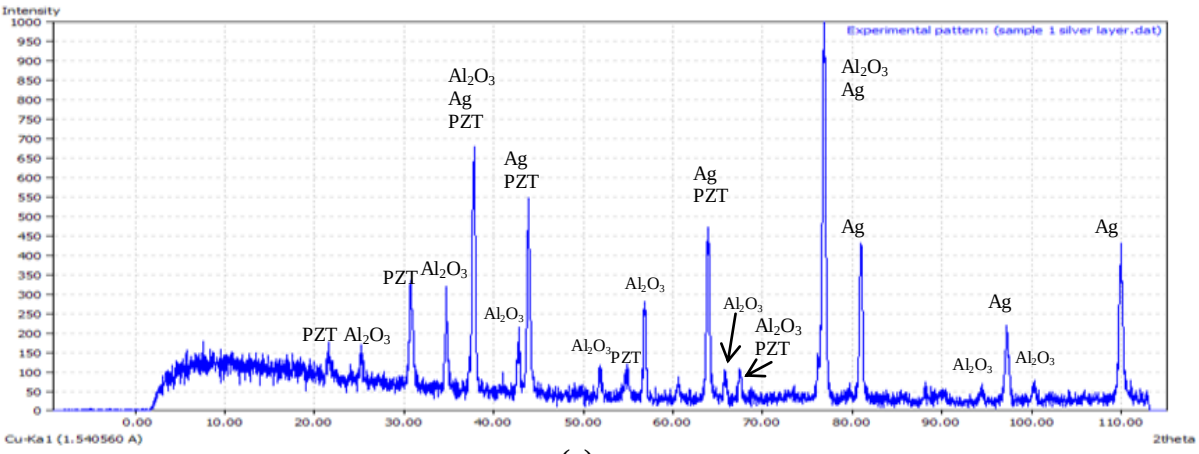

(c)

Figure 5.11: XRD patterns of (a) PZT powder (b) a thick-film sample (Si/Ag/PZT/Au) and (c) a thick-film sample (Al_2O_3/Ag/PZT/Ag). In the pattern of PZT powder (a), the peaks are labelled with corresponding Miller indices of pervoskite crystallographic planes. In the patterns of thick-film samples (b) and (c), each peak is labelled with material(s) which contribute to the peak. A peak may be a superimposition of peaks of several materials.

All the peaks of the thick-film samples find their sources from the starting component materials. There is no new phase found in the XRD patterns. However, considering XRD analysis usually can not detect a phase of below 5% of the total mass, a small amount of a lead silicate produced by the diffusive reaction between lead and silicon may be present but can not be identified in the XRD patterns. The 1 wt% borosilicate glass can not be identified either because it is amorphous.

5.6 Suitability of thick-film PZT on silicon for the MOA application

Due to the substrate clamping effect and the diffusion of lead to silicon, the d_{33} value (76 pC/N) of thick-film PZT on silicon is much lower than that of bulk PZT-5H (593 pC/N). The former is about 13% of the latter. As the bulk PZT-5H could bend the MOA test device to a radius of curvature (ROC) of 5 cm, it is estimated that thick-film PZT can bend the device to a ROC of 38 cm which is beyond the aim ROC of 5 cm. Thick-film PZT already made in this study can not provide enough actuation for the application. But all these thick-film PZT were single-layer PZT. Multiple layers of PZT can be deposited and may produce larger actuation than single-layer PZT and therefore may be suitable for the MOA application.

Chapter 6 CONCLUSIONS AND FURTHER WORK

From the experimental results and discussion presented in Chapter 5, the following conclusions can be made:

(1) Thick-film PZT samples with piezoelectric properties can be successfully made on silicon substrates. The thick-film PZT made has an average d_{33} of 76 pC/N. Its relative permittivity is 628. The whole manufacturing process of thick-film PZT samples was demonstrated to be successful, including wet ball-milling of starting powders, three roll milling of paste, doctor blading method, the sintering regime and oil bath poling.

(2) The sintering temperature from 850 ℃ to 950 ℃ does not have obvious effect on the piezoelectric properties of thick-film PZT on silicon.

(3) Wet ball-milling is necessary in the processing of starting powders because it greatly reduces the agglomerate size, tightens the particle size distribution and thus promotes sintering and homogeneity of thick-film PZT. This is demonstrated by the comparison between samples made using wet ball-milled powders and dry ball-milled powders.

(4) Piezoelectric properties of thick-film PZT on silicon substrates are not as good as those on alumina substrates. Thick-film on silicon substrates has an average d_{33} of 76 pC/N, while its counterpart on alumina substrates has a value of 120 pC/N.

(5) No reaction products in thick-film PZT sample on silicon substrates can be found to be generated during the sintering process in the XRD patterns. But this can not eliminate the possibility of the presence of a small amount of lead silicate (below 5 wt%).

(6) A single layer of thick-film PZT made by doctor blading method can not provide enough actuation for the MOA application.

In terms of further work, thick-film samples of multiple layers of PZT can be made to see if they have better piezoelectric properties than single-layer PZT. In addition, the thickness of the silicon substrate in the MOA could be decreased so the required actuation for the bending of MOA would be decreased. Moreover, as the silicon substrate has an adverse effect on the piezoelectric properties of PZT, a barrier layer between the PZT and the silicon could be tested. A platinised silicon substrate has a platinum thin film on silicon, which could act as a barrier layer and could have good adhesion to PZT.

References

1. Sanmartin, D.R., *Smart Piezoelectric devices for X-ray optics applications (PhD thesis)*, in *School of Metallurgy and Materials*. 2011, University of Birmingham: Birmingham.
2. Moulson, A.J. and J.M. Herbert, *Electroceramics*. 1990: Chapman and Hall.
3. Merz, W.J., *Domain formation and domain wall motions in ferroelectric $BaTiO_3$ single crystals.* Physical Review, 1954. **95**(3): p. 690-698.
4. Bouzid, A., et al., *PZT phase diagram determination by measurement of elastic moduli.* Journal of the European Ceramic Society, 2005. **25**(13): p. 3213-3221.
5. Southin, J.E.A., et al., *e(31),(f) determination for PZT films using a conventional 'd(33)' meter.* Journal of Physics D-Applied Physics, 2001. **34**(10): p. 1456-1460.
6. Dorey, R.A. and R.W. Whatmore, *Apparent reduction in the value of the d(33) piezoelectric coefficient in PZT thick films.* Integrated Ferroelectrics, 2002. **50**: p. 111-119.
7. Torah, R.N., S.P. Beeby, and N.M. White, *Experimental investigation into the effect of substrate clamping on the piezoelectric behaviour of thick-film PZT elements.* Journal of Physics D-Applied Physics, 2004. **37**(7): p. 1074-1078.
8. Torah, R.N., S.P. Beeby, and N.M. White, *Improving the piezoelectric properties of thick-film PZT: the influence of paste composition, powder milling process and electrode material.* Sensors and Actuators a-Physical, 2004. **110**(1-3): p. 378-384.
9. Glynne-Jones, P., et al., *An investigation into the effect of modified firing profiles on the piezoelectric properties of thick-film PZT layers on silicon.* Measurement Science & Technology, 2000. **11**(5): p. 526-531.
10. Chen, H.D., et al., *Dielectric, ferroelectric, and piezoelectric properties of lead-zirconate-titanate thick-films on silicon substrates.* Journal of Applied Physics, 1995. **77**(7): p. 3349-3353.
11. White, N.M. and J.D. Turner, *Thick-film sensors: Past, present and future.* Measurement Science & Technology, 1997. **8**(1): p. 1-20.
12. Baudry, H. *Screen-printing piezoelectric devices*. in *Proceedings of the sixth European Microelectronics Conference*. 1987.
13. Torah, R.N., et al., *Thick-film piezoceramics and devices.* Journal of Electroceramics, 2007. **19**(1): p. 97-112.
14. Beeby, S.P. and N.M. White, *Silicon micromechanical resonator with thick-film printed vibration excitation and detection mechanisms.* Sensors and Actuators a-Physical, 2001. **88**(3): p. 189-197.
15. Futakuchi, T., H. Yamano, and M. Adachi, *Preparation of ferroelectric thick film actuator on silicon substrate by screen-printing.* Japanese Journal of Applied Physics Part 1-Regular Papers Short Notes & Review Papers, 2001. **40**(9B): p. 5687-5689.
16. Dargahi, J., *A piezoelectric tactile sensor with three sensing elements for robotic, endoscopic and prosthetic applications.* Sensors and Actuators a-Physical, 2000. **80**(1): p. 23-30.
17. Maas, R., et al., *Thick-film printing of PZT onto silicon.* Materials Letters, 1997. **31**(1-2): p. 109-112.
18. Frood, A.J.M., et al., *Photoresist patterned thick-film piezoelectric elements on silicon.* Journal of Electroceramics, 2007. **19**(4): p. 327-331.

19. Thiele, E.S., D. Damjanovic, and N. Setter, *Processing and properties of screen-printed lead zirconate titanate piezoelectric thick films on electroded silicon.* Journal of the American Ceramic Society, 2001. **84**(12): p. 2863-2868.
20. Crescini, D., et al., *Large bandwidth and thermal compensated piezoelectric thick-film acceleration transducer.* Sensors and Actuators a-Physical, 2001. **87**(3): p. 131-138.
21. Beeby, S.P., N. Ross, and N.M. White, *Thick film PZT/micromachined silicon accelerometer.* Electronics Letters, 1999. **35**(23): p. 2060-2062.
22. de Reus, R., J.O. Gullov, and P.R. Scheeper, *Fabrication and characterization of a piezoelectric accelerometer.* Journal of Micromechanics and Microengineering, 1999. **9**(2): p. 123-126.
23. Koch, M., et al., *A novel micropump design with thick-film piezoelectric actuation.* Measurement Science & Technology, 1997. **8**(1): p. 49-57.
24. MacDonald, C.A. and W.M. Gibson, *Applications and advances in polycapillary optics.* X-Ray Spectrometry, 2003. **32**(3): p. 258-268.
25. Price, G.J., et al., *Hard X-ray imaging with microchannel plate optics.* Nuclear Instruments & Methods in Physics Research Section a-Accelerators Spectrometers Detectors and Associated Equipment, 2002. **490**(1-2): p. 290-298.
26. Willingale, R., C. Feldman, and A. Michette, *Active Microstructured Optical Arrays of Grazing Incidence Reflectors.* X-Ray Optics and Instrumentation, 2010. **2010**: p. 15.
27. Michette, A.G., et al., *Active microstructured x-ray optical arrays*, in *Euv and X-Ray Optics: Synergy between Laboratory and Space*, R. Hudec and L. Pina, Editors. 2009, Spie-Int Soc Optical Engineering: Bellingham.
28. Michette, A.G., et al., *Smart X-Ray Optics*, in *9th International Conference on X-Ray Microscopy*, C. David, et al., Editors. 2009, Iop Publishing Ltd: Bristol.
29. Dunare, C., et al., *Micromachining Optical Arrays*, in *International Conference of Semiconductors*. 2010: Sinaia, Romania.
30. Michette, A., et al., *Active micro-structured arrays for X-ray optics - art. no. 670502*, in *Advances in X-Ray/Euv Optics and Components Ii*, A.M. Khounsary, C. Morawe, and S. Goto, Editors. 2007, Spie-Int Soc Optical Engineering: Bellingham. p. 70502-70502.
31. Sanmartin, D.R., et al., *Progress on the development of active micro-structured optical arrays for X-ray optics*, in *Advances in X-Ray/Euv Optics and Components Iv*, A.M. Khounsary, C. Morawe, and S. Goto, Editors. 2009, Spie-Int Soc Optical Engineering: Bellingham.
32. Sanmartin, D.R., et al., *Development of spider micro-structured optical arrays for X-ray optics*, in *Adaptive X-Ray Optics*, A.M. Khounsary, S.L. Odell, and S.R. Restaino, Editors. 2010, Spie-Int Soc Optical Engineering: Bellingham.
33. Dunare, C., et al., *Microstructured Optical Arrays for Smart X-ray Optics*, in *Euv and X-Ray Optics: Synergy between Laboratory and Space*, R. Hudec and L. Pina, Editors. 2009, Spie-Int Soc Optical Engineering: Bellingham.
34. Cotton, D.P.J., et al., *A new binderless thick-film piezoelectric paste.* Journal of Materials Science-Materials in Electronics, 2007. **18**(10): p. 1037-1044.
35. Das, R.N., A. Pathak, and P. Pramanik, *Low-temperature preparation of nanocrystalline lead zirconate titanate and lead lanthanum zirconate titanate powders using triethanolamine.* Journal of the American Ceramic Society, 1998. **81**(12): p. 3357-3360.

36. Haigh, R.D. and R.W. Whatmore, *On the processing conditions and interfacial chemistry of composite PZT thick films on platinised silicon substrates.* Sensors and Actuators a-Physical, 2009. **151**(2): p. 203-212.